

Acknowledgement

I thankin fact there are a lot of persons and institutions that contribute to my academic career. Firstly, I am grateful with my parents, brothers and aunt since they supported me what they could do and inspired me to pursuit those impossible things that I never thought to achieve. Secondly, I'm grateful with the Hybrid Tailored System group at University of Vienna, Carlos, Toma and Paola.....you have allowed me to understand why the carbon nanotubes are extremely difficult to produce and the physics theory behind of it. Thirdly, I am grateful with University of Vienna because they provided me the best quality of physicists, chemists and great professionals in many areas to improve my academic qualifications in order to contribute to this society. And many others...thank you so much.....

Finally, I thank COLFUTURO for providing the financial means, which have made possible the participation of the Master of Science Program at the University of Vienna.

Gracias Dios por abrirme este espacio en el albúm de mi vida. Recordaré los buenos y difciles momentos que pasé, los cuales me muestra de lo que soy capaz.....Paola, a ti gracias por la oportunidad!!!!

Abstract

The following Master thesis focuses on the study of the optical response of boron doped single-walled carbon nanotubes. Boron is one of the natural dopants for SWCNTs, because of its size proximity to carbon. However, the synthesis of such materials has been hindered for several years compared to the carbon pristine counterparts. In this MsSc thesis I focus on the study of B doped single walled carbon nanotubes (CBx-SWCNTs).

In general, producing doped nanotubes with the already standard techniques for the growth of pristine carbon tubes requires fine control of different parameters. Arc discharge and laser ablation were the first techniques to accomplish the synthesis of CBx-SWCNTs. However, the particular case of chemical vapor deposition was extremely difficult for several years requires very careful experimental adjustments. Using the same type of catalysts for the growth of pristine C (a), N-doped (b) or B-doped (c) can give radically different results using the same technique. This means that in the three corresponding situations, high yield of SWCNTs, growth of multiwalled tubes exclusively and no growth of tubes can actually happen using the same catalyst.

The synthesis method used in this thesis was high vacuum chemical vapor deposition (HV-CVD), which is a method developed in the group that hosted this work. This technique can allow the use of a single liquid feedstock containing the carbon precursor and boron heteroatoms. The CBx-SWCNTs grown by this method have the peculiarity to grow within a very narrow diameter distribution window. However, in the preceding investigations, this material had only been characterized regarding B and bonding environments in as-grown samples. A further study with optical techniques of the same material and purified samples was lacking. The purpose of this thesis is to inspect the optical properties of this novel material making use of Raman spectroscopy, optical absorption spectroscopy and photoluminescence. These techniques are ideal to identify the tubes' properties because they exhibit selective optical absorption transitions, an ultra-sensitive resonance Raman response and their quantum yield in photoluminescence is remarkable.

This master thesis is divided into four chapters: the first one provides an overview of the theoretical background behind the structural correlation between single-walled carbon nanotubes and their electronic and optical properties. Chapter 2 focuses on the material production and characterization methods. In Chapter 3 I have summarized the experimental part of my work to finalize in Chapter 4 with a discussion of the results obtained. A section with concluding remarks and perspectives is included at the end of this work.

Zusammenfassung

Diese Master-Arbeit befasst sich mit der Untersuchung der optischen Eigenschaften von Bor-dotierten einwandigen Kohlenstoff-Nanoröhren (SWCNT). Bor ist, aufgrund der geringen Größenunterschiede zwischen Bor- und Kohlenstoffatomen, eine der natürlichen Dotierungssubstanzen für SWCNT. Dennoch gestaltete sich die Herstellung solcher B-dotierter SWCNT (CBx-SWCNT) bisher sehr schwierig. Deshalb liegt der Schwerpunkt dieser Arbeit in der Charakterisierung von CBx-SWCNT.

Generell erfordert die Produktion von dotierten SWCNT mittels Standard-Verfahren die präzise Kontrolle verschiedener Parameter während des Herstellungs-Prozesses. Während die Lichtbogen-Verdampfungs-Technik und die Laserablations-Technik erfolgreich zur Herstellung von CBx-SWCNT benutzt wurden, ist die Produktion mittels chemischer Gasphasenabscheidung schwieriger. Trotz Verwendung desselben Katalysators, kann die Herstellung von undotierten, Stickstoff-dotierten und Bor-dotierten SWCNT zu sehr unterschiedlichen Resultaten führen, wie zum Beispiel dem Wachstum einer großen Anzahl von undotierten SWCNT, dem Wachstum von mehrwandigen Kohlenstoff-Nanoröhren oder keinem Nanoröhren-Wachstum.

Chemische Gasphasenabscheidung im Hochvakuum wurde als Herstellungsmethode für die CBx-SWCNT in dieser Arbeit verwendet. Diese Technik erlaubt die Verwendung einer flüssigen Kohlenstoff-Quelle, welche gleichzeitig auch die Bor-Heteroatome enthält. Mittels dieser Methode wurden CBx-SWCNT Strukturen mit sehr enger Durchmesser-Verteilung erzeugt. Diese Proben wurden zuvor nur im ungereinigten Zustand erforscht, wohingegen im Rahmen dieser Studie vor allem gereinigte CBx-SWCNT untersucht wurden. Diese Untersuchungen wurden mittels Raman-Spektroskopie, Optischer-Absorptionsspektroskopie, sowie Photolumineszenz-Spektroskopie durchgeführt, welche sich besonders für diese Studien eignen, aufgrund der einzigartigen Signatur von CBx-SWCNT in optischer Absorption und Raman.

Diese Master-Arbeit ist in vier Kapitel unterteilt: Das erste Kapitel enthält einen Überblick über den theoretischen Hintergrund der elektronischen und optischen Eigenschaften von Kohlenstoff-Nanoröhren. Das zweite Kapitel erklärt die Herstellung und Charakterisierung der CBx-SWCNT Proben. In Kapitel 3 werden die experimentellen Resultate präsentiert, welche in Kapitel 4 ausführlicher diskutiert werden. Am Ende dieser Arbeit findet sich ein Kapitel mit abschließenden Bemerkungen und Schlussfolgerungen.

Contents

1	Introduction	1
2	Theoretical background	3
2.1	Carbon features and its allotropes	4
2.2	Properties of SWCNTs	5
2.2.1	Electronic structure of SWCNTs	5
2.2.2	Tight-binding model	9
2.2.3	The Zone-Folding approximation	11
2.2.4	Density of states (DOS)	12
2.2.5	Optical properties	14
2.3	Substitutional doping	17
2.3.1	High doping and Low doping	18
2.3.2	B-doped nanotubes: ultra-low doping	19
3	Methods	20
3.1	Material Production Methods	20
3.1.1	Electric Arc Discharge	21
3.1.2	Laser ablation	22
3.1.3	Chemical vapor deposition	23
3.1.4	High Vacuum Chemical Vapor Deposition	23
3.2	Optical Characterization methods	24
3.2.1	Raman spectroscopy	25
3.2.2	Optical absorption spectroscopy	27
3.2.3	Photoluminescence spectroscopy	28
4	Production of CB_x-SWNTs	31
4.1	Growing process of CB _x -SWNTs	31
4.2	Purification process	34
5	Optical Characterization of CB_x-SWNTs	36
5.1	Raman spectroscopy results	36
5.2	FT-Raman spectroscopy results	42
5.3	Optical absorption spectroscopy results	43
5.4	Photoluminescence spectroscopy	45
5.5	Final comments	47
	Bibliography	51

Chapter 1

Introduction

Single-walled carbon nanotubes (SWCNTs) are tubular structures that exhibit remarkable electronic and mechanical properties which strongly depend on their diameter and chirality[1–8]. Up to now, several experimental methods have been studied to control their properties for different applications. One of such methods is substitutional doping of heteroatoms such as B (Boron), N (Nitrogen), or P (Phosphorus).

For a SWCNT to grow, a carbon precursor is necessary for the process. This precursor could contain just carbon, or also additional heteroatoms like nitrogen or boron among others. A carbon nanotube where carbon atoms are directly replaced by heteroatoms is seen as a substitutionally doped tube. Figure 1.1 shows a substitutional N atom in a graphitic network (taken from reference [2]).

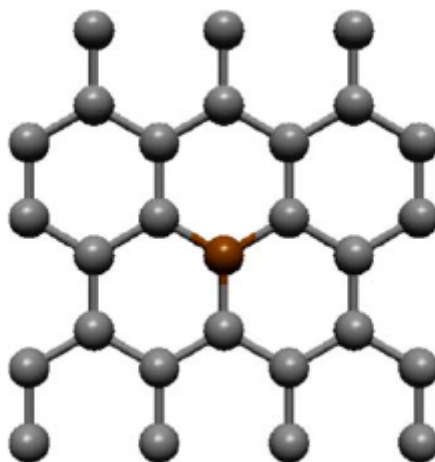


Figure 1.1: Substitutional atom in a graphitic network. The grey atoms represent carbon while the brown represents the substitutional heteroatom (in this case a N atom). Reproduced and modified from [2]

The substitutional atoms can behave as *donors* or *acceptors*. Thus, while the metallic and semiconducting character of SWCNTs depends on their diameter and chirality, the inclusion of heteroatoms into their structure can modify their electronic properties. Doing this in a controlled manner is particularly appealing for different applications. In order to produce doped SWCNTs, several experiments which involve high temperatures like electric arc discharge, laser ablation chemical vapor deposition have been proposed [9–12]. However, for the case of boron-doped SWCNTs (CBx-SWNTs), a limited number of publications are available in the literature. As mentioned above, modifying systems tuned for the synthesis of pristine material is not a trivial task. McGuire et al.[13] published one of the first experimental results suggesting that CBx-SWNTs exhibit different electronic and structural properties due to the boron presence into the carbon network. In particular, using chemical vapor deposition are particularly limited because of high contamination of the catalysts and the instability of the synthesis reactors due to the diffusion of elemental boron through the interstitials of the materials from which the reactors are made. This can cause the synthesis apparatuses to collapse at elevated temperatures.

In the particular case of this thesis, a modified high-vacuum CVD system was used. In this case a feedstock with carbon and boron on the same chemical compound is used. [2, 3, 14]. Results reported on CBx-SWNTs grown with this method describe the production of tubes with small diameters and a narrow diameter distribution about 0.9 and 1.5nm. Additionally, the group where I have done my work has developed a method to purify doped tubes by means of an adapted ultracentrifugation method, which allows identifying the factual the doping level or dopant concentration in the in a bare nanotube sample. Although some studies of the optical response of CBx-SWNTs have been done on raw arc-discharge material, [15], given that these purification results on CBx-SWNTs produced by HV-CVD are so recent, no studies of the optical properties of this interesting material are available.

In this context, the present master thesis has focused on the production of CBx-SWNTs with new catalysts in HV-CVD. To explore the optical properties of these CBx-SWNTs, Raman, optical absorption and photoluminescence spectroscopies have been used as probing techniques [16–18]. The research is part of the ongoing investigations of **the Hybrid Tailored Structures group** at the University of Vienna. This group has designed a promising technique that will enable the production of clean and metallicity sorted CBx-SWNTs at large scale.

Chapter 2

Theoretical background

In 1991, SWCNTs were for the first time observed by Iijima at NEC Laboratories in Japan using high-resolution transmission electron microscopy (HRTEM) [19]. The results revealed the chiral and tubular structure of SWCNTs, and allowed the description of their electronic properties. Since then, SWCNTs research has been followed by reports on remarkable applications. To understand what SWCNTs are, it is necessary to refer to their elemental composition. Basically, SWCNTs are composed of carbon atoms and if the tubular structure was unrolled, it would look like a graphene sheet, which is hexagonal arrangement of carbon atoms. Since the electrons in both SWCNTs and graphene have the similar local atomic distribution, the electronic structure of a nanotube can be inferred from that of its parent material.

From the valence and conduction bands that can be computed for nanotubes, they outstandingly reveal **semiconducting** and **metallic** character which is truly and only dependent of the carbon atom arrangement. Thence, the corresponding features in the electronic density of have stimulated further research on diverse applications in electronics, engineering and other related fields. Nanotubes also exhibit outstanding optical and mechanical properties.

This chapter provides the theoretical background to understand the outstanding electronic and optical properties that nanotubes have. The starting point is a brief review of the main element of single-walled nanotubes: carbon. Taking into account the element carbon and more precisely the electronic structure of **graphene**, I will describe their electronic properties using some theoretical elements from solid state physics. Finally, the optical responses of SWCNTs will be described.

2.1 Carbon features and its allotropes

The fundamental element of SWCNTs is carbon. This element is the most abundant on the planet Earth and it sustains several organic processes owing to its wide range of possibilities to form different chemical bondings with other atoms; therefore it is responsible for life on our planet [20]. The electronic structure of carbon plays an important role in how it forms different chemical bonds. As consequence, diverse carbon species known as allotropes (fullerenes, diamond, and others) exhibit particular properties. Although there are several amorphous forms of carbon, the allotropes are characterized by a covalent bonding. Essentially, the covalent bonding describes how the carbon atoms share electrons between each other and implicitly how electrons will occupy a determined energy level [21, 22]. Consequently, the carbon atom exhibit the bonding and antibonding states, which they allow to form orbital hybridizations of carbon (sp^n)

The sp^n hybridization describes how the electrons in carbon are organized per orbital and energy level (n and sp respectively). The type of hybrid orbital sp^n provides information of its shape and direction and it allows inferring the types of bonding between carbon atoms that are possible. A pure s orbital has a sphere shape whereas p has lobular shape (direction on x, y, z). Regarding the index n , it has three values related with energy and orbital level (Table 2.1).

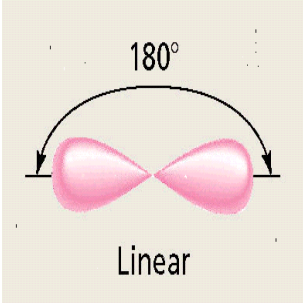
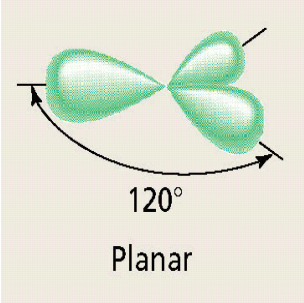
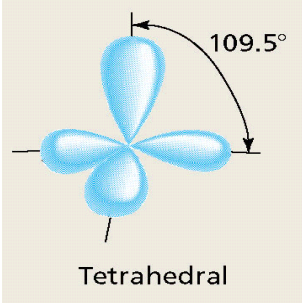
		
sp^1	sp^2	sp^3
Acetylene, Carbyne	Ethene, SWCNT's, graphene	Diamond, Ethane, Methane

Table 2.1: Orbital hybridization sp^m on Carbon and their shapes. Reproduced and modified by [23]

The shape and direction of the orbital determine the type of bonding states for carbon. Thus, the lobes which overlap on planar-like to internuclear axis are called σ bonds. The σ -bond contributes to determine the mechanical properties of carbon materials, while a π -bond contributes to determine its electronic properties of carbon given that this bond is close to the Fermi level [6]. Clearly, the Orbital

Hybridizations in carbon play an important role to explore their the electronic structure which yields measuring optical, magnetic, and electrical properties.

2.2 Properties of SWCNTs

The SWCNTs can be pictured as a graphene sheet rolled up to form a cylindrical structure. This cylindrical structure has a periodic arrangement of atoms in a hexagonal lattice. The theoretical formalism of solid state physics usually describes the graphene sheet using lattice vectors point of view [24]. The unit lattice vectors and their algebra analyzed in real and reciprocal space, provides information regarding the electronic properties of SWCNTs. The semiconducting or metallic character of SWCNTs depends of the occupation of energy levels in the valence and conduction bands. However, due to their one dimensionality, nanotubes exhibit van Hove singularities in their joint density of states. In order to briefly describe this features a tight-binding and zone-folding models will be briefly introduced below. These aspects will also contribute to describe the optical properties of SWCNTs.

2.2.1 Electronic structure of SWCNTs

A single layer of graphene is related to SWCNTs because both exhibit the same orbital hybridization sp^2 . Thus, the lattice vectors of SWCNTs can be described as the graphene lattice vectors (\vec{a}_1, \vec{a}_2) . **The Chiral vector** \vec{C}_h describes the direction in which a graphene sheet would be rolled up to form a certain SWCNT, and it is given by

$$\vec{C}_h \equiv n\vec{a}_1 + m\vec{a}_2, \quad (2.1)$$

Where the indices (n, m) are the indices of the linear combination of the lattice vector, which in turn allow do describe the structure and electronic properties of a SWCNT [6]. Geometrically speaking, the chiral vector is related to the circumference of the cylindrical structure of SWCNTs. In Cartesian components, the vectors \vec{a}_1 and \vec{a}_2 are derived by geometry.

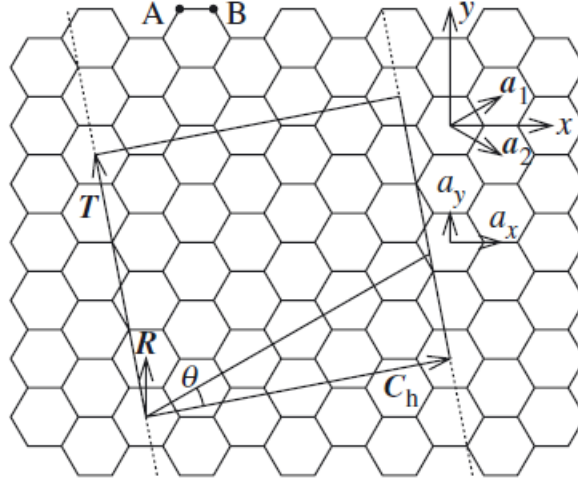


Figure 2.1: Lattice unit vectors in Cartesian components. Reproduced from [5]

The Cartesian components of the unit vectors are:

$$a_x = \sqrt{3} \cos(30^\circ) = \frac{3}{2} \quad a_y = \sqrt{3} \sin(30^\circ) = \frac{\sqrt{3}}{2},$$

Hence,

$$\vec{a}_1 = \left(\frac{\sqrt{3}}{2}, \frac{1}{2} \right) a, \quad (2.2)$$

$$\vec{a}_2 = \left(\frac{\sqrt{3}}{2}, -\frac{1}{2} \right) a,$$

where $a = \sqrt{3}a_{cc}$ is the lattice constant and a_{cc} is C-C bond length whose value is approximately 1.42\AA . This determines the magnitude of the chiral vector \vec{C}_h as,

$$|\vec{C}_h| = \sqrt{3}\sqrt{n^2 + nm + m^2}, \quad (2.3)$$

recalling that the chiral vector \vec{C}_h is related to the circumference of SWCNTs. The tube diameter is given by

$$d_T = \frac{C_h}{\pi} = \frac{\sqrt{3}a_{cc}\sqrt{n^2 + nm + m^2}}{\pi}, \quad (2.4)$$

On the other hand, the projection of \vec{C}_h onto \vec{a}_i (with $i = x, y$), gives the angle at which the SWCNTs structure is rolled up as

$$\vec{C}_h \cdot \vec{a}_i = |\vec{C}_h| |\vec{a}_i| \cos \theta,$$

As a result of the projection, the **chiral angle** θ is deduced in terms of lattice components (n, m) as

$$\theta = \cos^{-1} \left(\frac{2n + m}{2\sqrt{n^2 + nm - m^2}} \right), \quad (2.5)$$

Accordingly with the Figure 2.1, the chiral angle has an interval of $0 \leq \theta \leq 30^\circ$ which defines the types of nanotubes as follows:

- If $n = m$ and $\theta = 30^\circ$ the nanotube circumference has an armchair form
- If $m = 0$, $\theta = 0^\circ$ the nanotube circumference has a zigzag form
- If $n \neq m \neq 0$ the nanotube circumference has an achiral form.

Notation	Meaning	Equation	Magnitude
a	lattice constant	$a = \sqrt{3}a_{cc}$	$a_{cc} = 1.42 \text{ \AA}$
\vec{a}_1, \vec{a}_2	lattice vectors	$(\frac{\sqrt{3}}{2}, \frac{1}{2})a; (\frac{\sqrt{3}}{2}, -\frac{1}{2})a$	a
\vec{b}_1, \vec{b}_2	Reciprocal vectors	$(\frac{1}{2}, \frac{\sqrt{3}}{2}); (\frac{1}{2}, -\frac{\sqrt{3}}{2})$	$ \vec{b} = \frac{4\pi}{\sqrt{3}a}$
θ	chiral angle	$\theta = \cos^{-1}(\frac{2n+m}{2\sqrt{n^2+mn-m^2}})$	$\tan \theta = \frac{\sqrt{3}m}{2n+m}$
$n = m$	Armchair	$ C_h = 3n$	
$m = 0$	Zigzag	$ C_h = \sqrt{3}n$	

Table 2.2: Main features of SWCNTs

Table 2.2 summarizes the SWCNT features. The diameter d_T and chiral angle θ are the crucial elements to elucidate the SWCNTs' electronic properties. The analysis of the SWCNTs' lattice in reciprocal space provides additional information about the semiconducting and metallic character of the nanotubes. Essentially, the reciprocal space (k -space) describes the diffraction phenomena for any periodic lattice [25]. In Figure 2.2, the vectors \vec{b}_1 and \vec{b}_2 represent the unit cell in the reciprocal space and define the lattice in the first Brillouin zone (BZ).

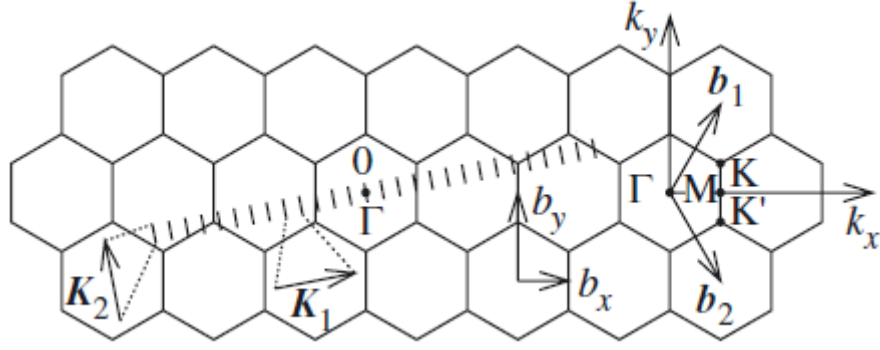


Figure 2.2: Reciprocal space vector and the first Brillouin zone. From[5]

Additionally, the Figure 2.2, the first Brillouin zone forms a hexagon, which exhibits high-symmetry points on Γ , K , K' and M [6]. Thus, Γ represents the center of the hexagonal lattice, while $K - M - K'$ are periodic distances in the lattice.

The vectors (\vec{b}_1, \vec{b}_2) can also be written by Cartesian components;

$$\begin{aligned}\vec{b}_1 &= \left(\frac{1}{\sqrt{3}}, 1 \right) \frac{2\pi}{a_0}, \\ \vec{b}_2 &= \left(\frac{1}{\sqrt{3}}, -1 \right) \frac{2\pi}{a_0},\end{aligned}\tag{2.6}$$

where $\frac{2\pi}{a_0}$ corresponds to the lattice constant on reciprocal space. That lattice constant defines the reciprocal lattice vector on the tube axis in z-direction (\vec{k}_z) perpendicular to (\vec{b}_1, \vec{b}_2) . The length of such vector is written as,

$$k_z \equiv \frac{2\pi}{a_0},$$

This relation suggests the nanotube is infinitely long, then the wave number k_z is continuous on the interval $\left(-\frac{\pi}{a_0}, \frac{\pi}{a_0}\right)$. Moreover, any vector on reciprocal space perpendicular to the chiral vector \vec{C}_h is the perimeter of the circumference in the nanotube, which is quantized under the following boundary conditions;

$$\vec{k}_{\perp,m} = \begin{cases} |\vec{C}_h| = \pi \cdot d_T = \lambda \cdot m \\ k_{\perp,m} = \frac{2\pi}{\lambda} = \frac{2m}{d_T}, \quad \frac{q}{2} + 1, \dots, 0, 1, \dots, \frac{q}{2} \end{cases}$$

m takes integer numbers where the wave function of the electron in the graphene undergoes a phase shift around the circumference owing to $2\pi m$ and therefore, the all others wavelengths would vanish by interference [24]. The maximum or minimum of wavelengths for the wave vector $\vec{k}_{\perp,m}$ determine which wavelengths and energies are allowed or forbidden in the first Brillouin zone. Additionally, q represents the lines parallel to z-axis separated by interval $\left(-\frac{\pi}{a_0}, \frac{\pi}{a_0}\right)$ and $\vec{k}_{\perp} = \frac{2}{d_T}$.

In order to derive the allowed wavelengths and energies in the BZ of the graphene, it is necessary two theoretical descriptions: Tight-binding and Zone-Folding.

2.2.2 Tight-binding model

The σ and π bondings determine the properties of a carbon nanotube. The σ -bond determines the mechanical properties but it does take part of chemical reactions. On the other hand, the π -bond happens with the atoms that are not responsible of the lattice bonding. Thus they are responsible for the good electrical conductivity and chemical reactions. These differences between π and σ bonds are crucial to characterize the electronic band structure of graphene. Under these conditions, the energies allowed in the first BZ of graphene in π -bond have the form,

$$E^{\pm}(k_1, k_2) = \frac{\varepsilon_{2p} \pm \gamma_0 \sqrt{f_{12}(k_1, k_2)}}{1 \pm s_0 \sqrt{f_{12}(k_1, k_2)}} \quad (2.7)$$

This relation represents the allowed energies in the first BZ regard to the high symmetric points (Γ , K , M , K'). The terms ε_{2p} , γ_0 , and s_0 are empirical parameters of the band structure in graphene. At the K -point, the term $(k_1 = \frac{1}{3}, k_2 = -\frac{1}{3})f_{12}$ vanishes. In this point, the π and π^* bands represent the conduction and valence band, respectively and the energy is set to zero in the Fermi level. At Γ -point, the π and π^* bands have a maximum and minimum energies as depicted in Figure 2.3.

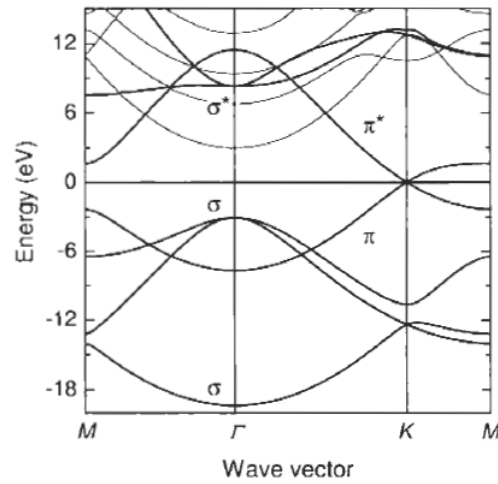


Figure 2.3: The electronic band structure of Graphene. Reproduced from Ref[26]

For metallic tubes, the first BZ is depicted by a hexagon with K' and K high symmetry points, wherein the π and π^* bands cross each other (Figure 2.4). If it magnifies the K' – *point* the valence and conduction band are distinguishable and indeed, for K – *point* happens the same situation. In that sense, the $K - K'$ points are equivalent in graphene and they are called Dirac points

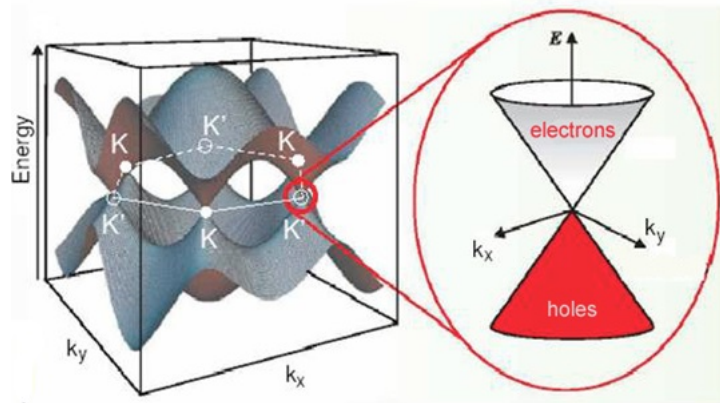


Figure 2.4: The electronic band structure of Graphene in 3D. Reproduced from Ref [27]

Taking into account the $K - K'$ high symmetry points, the electronic band structure in SWCNTs can be derived. The semiconducting and metallic character of a nanotube depends on additional boundary conditions, which define the difference between a SWCNT and graphene: its quantum confinement.

2.2.3 The Zone-Folding approximation

In order to determine the semiconducting and metallic character in SWCNTs, it is necessary to verify the allowed wave vectors \vec{K} or k - lines which cross the high-symmetry points Γ , K , K' and M in the reciprocal space under boundary conditions. Firstly, the equation 2.7 is constrained by $\vec{K} \cdot \vec{C}_h = 2\pi m$. This condition carries the possible projections of the wave vector \vec{k} around the chiral vector \vec{C}_h . And secondly, the K - point where π and π^* bands cross, they contribute for the metallic character in SWCNTs, i.e, the conduction and valence band have the approximate equal amount of electrons moving quasi-static free in a solid (Figure 2.5a).

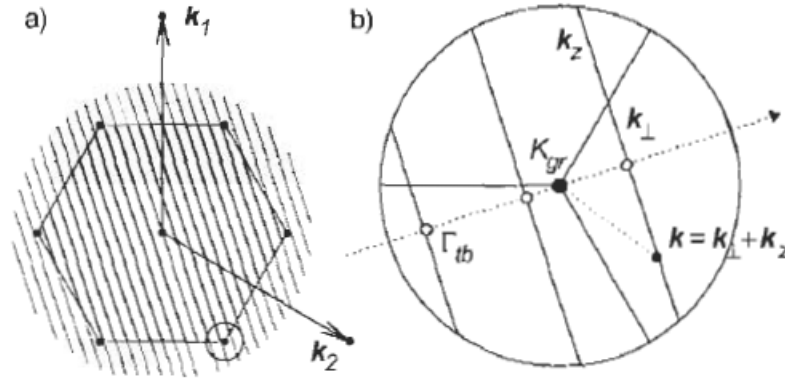


Figure 2.5: The allowed wave vectors in the first Brillouin zone. (a) In nanotubes where the allowed wave vectors cross the K - point show semiconducting character, (b) For the nanotubes where the wave vectors do not cross the K - point show metallic character in SWCNTs. Reproduced from Ref [26]

In Figure 2.5b, the slope in the k - lines are determined by the chiral symmetry [7]. The k - line length is $(\frac{2\pi}{a})$ and its distance between each other is $(\frac{2}{d_T})$. If the k - lines cross the K - point high symmetry, i.e, wherein π and π^* bands cross each other, the SWCNTs exhibit metallic character (Figure 2.5a). But, if the k - lines do not cross the K - point, the SWCNTs exhibit a semiconducting character (Figure 2.5b)

The k - lines could be projected in two directions: along of the tube structure in SWCNT k_z and around of the circumference of the tube k_\perp (Figure 2.5b). In direction of k_\perp discrete values are constrained under boundary conditions around chiral vector \vec{C}_h of the nanotube. On the other hand, in direction of k_z , there are continuous values because the tube is considered infinitely long [20]

According with these wave vectors \vec{k}_\perp and \vec{k}_z could find the following conditions:

$$\begin{aligned}\vec{k}_\perp \cdot \vec{C}_h &= 2\pi & \vec{k}_\perp \cdot \vec{a} &= 0 \\ \vec{k}_z \cdot \vec{C}_h &= 0 & \vec{k}_z \cdot \vec{a} &= 2\pi\end{aligned}\tag{2.8}$$

The direction of the wave vectors \vec{k}_\perp and \vec{k}_z contribute to the confinement condition, which is the fundamental idea of zone-folding approximation. The allowed (k - lines) generally are constrained by the condition $\vec{k}_\perp \cdot \vec{C}_h = 2\pi m$ for the nanotubes [26]. This condition yields

$$\vec{K} \cdot \vec{C}_h = \frac{2\pi}{3}(n - m)\tag{2.9}$$

Where $\vec{K} = \frac{1}{3}(\vec{k}_1 - \vec{k}_2)$, thus,

$$\vec{K} \cdot \vec{C}_h = \frac{1}{3}(\vec{k}_1 + \vec{k}_2) \cdot \vec{C}_h = \frac{2\pi}{3}(n - m)\tag{2.10}$$

The nanotube is a metallic if $n - m = 3l$, i.e, whether $n - m$ is a multiple of three. On the other hand, the nanotube is semiconducting if $n - m \neq 3l$. Taking this as rough estimate, it is easy to infer that most carbon nanotubes have semiconducting character whereas $\frac{1}{3}$ have metallic character [6]. Clearly, the zone folding approximation provides information regarding the semiconducting and metallic character in SWCNTs. However, this is confinement criteria are not sufficient condition to elucidate the differences between graphene and SWCNTs.

2.2.4 Density of states (DOS)

One of the differences between SWCNTs and graphene structures lie on their dimensionality. On the one hand, SWCNT is a structure oriented in three directions but only one is extended (1D) and on the other hand, graphene is a structure oriented in three directions but two of them are extended whereas the other is fixed (2D). The study of such remarkable difference between 1D and 2D structures is given by the density of states (DOS), which provides information of the electrons energies occupancy in the valence or conduction bands. The energy occupancy is remarkable different for 1D and 2D structures for graphene and SWCNTs.

The DOS is different for the structures with a particular dimensionality. Hence, the DOS for 2D-structures like graphene, picture energy peaks as step function, whereas the 1D-structures like SWCNTs, picture peaks a parabola function (Figure 2.6).

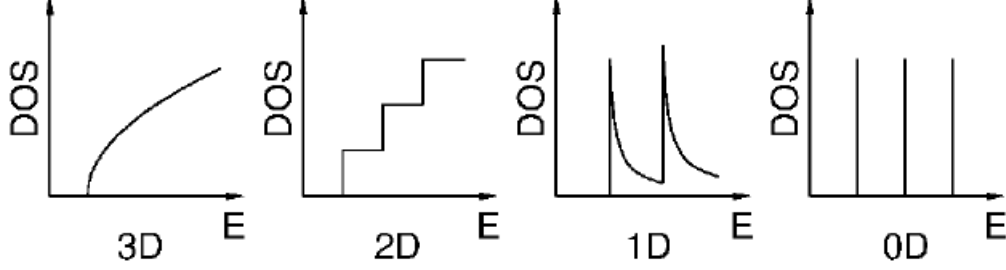


Figure 2.6: Density of States and its energy critical points (vHs) for any dimensionality. Reproduced from Ref [7]

For SWCNTs, the DOS is denoted by $n(E)$ and commonly it is defined as:

$$n(E) = \frac{2}{q|k_z|} \sum_i \int dk_z \delta(k_z - k_i) \left| \frac{\partial E^+(k_\perp, k_z)}{\partial k_z} \right|^{-1} \quad (2.11)$$

Each wave vector k_i is given by the energy $E - E^\pm(k_\perp, k_z) = 0$. The term $\frac{2}{q|k_z|}$ is the total area of the nanotube in the first BZ [26]. The corresponding derivative term $(\frac{\partial E^+(k_\perp, k_z)}{\partial k_z})$ is approximated to the electronic band structure as straight lines next to the K - point. With that, the DOS is given as,

$$n(E) = \frac{4a_0}{\pi^2 d \gamma_0} \sum_{m=-\infty}^{\infty} g(E, E_m) \quad (2.12)$$

The terms γ_0 and a_0 correspond to the carbon-carbon interaction energy and lattice unit, respectively. Likewise, $g(E, E_m)$ determines the energy peak like a step function with parabola shapes under the following cases:

$$g(E, E_m) = \begin{cases} \frac{|E|}{\sqrt{E^2 - E_m^2}} & |E| > |E_m| \\ 0 & |E| < |E_m| \end{cases}$$

For the case $E = E_m$, there is a critical point of energy, which is called **van Hove singularities**(vHs) and they are proportional to $(E^2 - E_m^2)^{-1/2}$ for both minimum

and maximum of energy (Figure 7b). For the case $E_m = 0$, the value of $g(E, 0)$ will be constant.

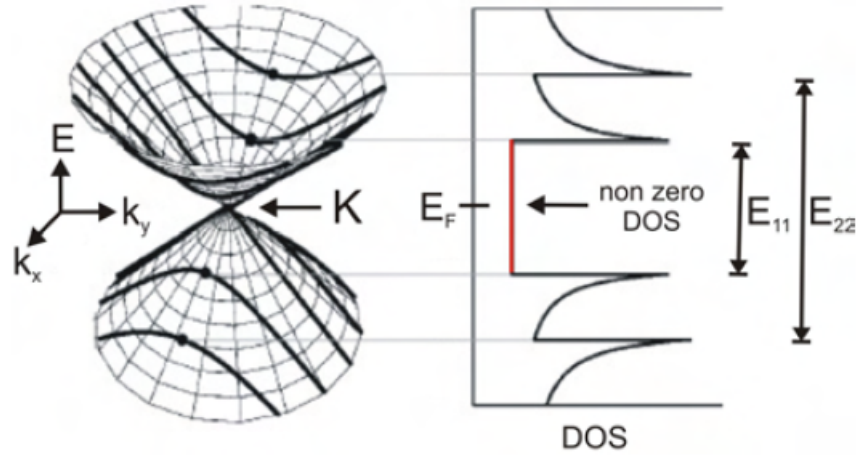


Figure 2.7: Density of States in a metallic SWCNT. (a) The bold lines represent the allowed wave vectors k – lines or cutting lines for a metallic SWCNT in the cone (b) The formation of the vHs connected by the cutting lines of the cone and its energy transitions. Reproduced from Ref [26]

With the cases of $g(E, E_m)$, the non-zero value of DOS at Fermi energy level (Figure 7b) represents the metallic feature for a nanotube. The DOS values are inverse proportional to the nanotube diameter ($DOS \propto \frac{1}{d_T}$). Conversely, the zero value of DOS at the Fermi energy level represents the semiconducting character of the the nanotube. The energy transitions of the electrons in π and π^* bands for 1D-structure, are depicted as peaks or vHs (Figure 2.7b). These energy transitions pictures the optical responses in SWCNTs. The energy transitions depicted as E_{11} and E_{22} correspond to the first and second pair of vHs for valence and conduction bands. Indeed, other types of energy transitions occurs, e.g, the E_{12} transition means that an electron changes its first energy level in valence band to the second energy in the conduction band. This is associated to the relative electric field polarization regard to the nanotube [28] Consequently, the energy transitions represent the optical responses in SWCNTs by means of DOS and their vHs. Both provide the optical properties for SWCNTs.

2.2.5 Optical properties

Understanding the optical properties of a SWCNT additionally allows exploring their electronic structure of SWCNTs. For instance, the absorption-emission spectra include the electronic transitions between the valence and conduction bands. These bands are analyzed from the density of states (DOS) and vHs.

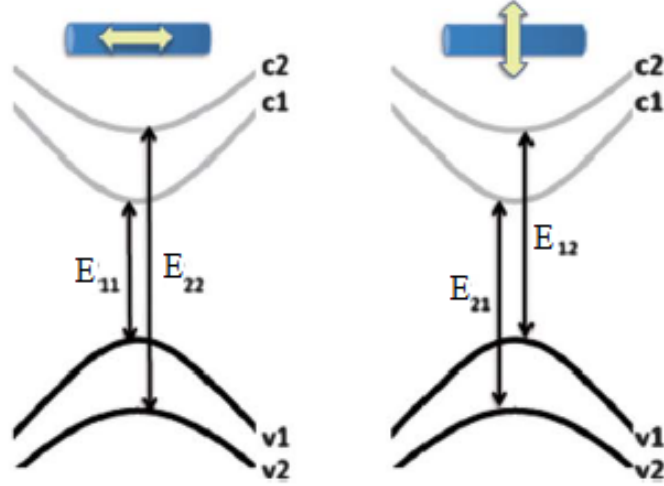


Figure 2.8: Electronic transitions in SWCNTs for optical excitations. C1 and C2 correspond to the first and second energy level in the conduction band respectively; in the same sense V1 and V2. Accordingly with the polarization of electric field vector along or perpendicular to the nanotube, the electronic transitions are different. Reproduced and modified from Ref [7]

In this sense, the optical responses are the interaction between light and matter by means of absorption, emission, reflection, and scattering phenomena. Generally, the polarization vector \vec{P} relates these phenomena, which is induced by external electric field \vec{E} [26]. In SWCNTs, when the light is absorbed by a nanotube, it obeys a selection rules that depend on the relative polarization of the electric field vector regard to the nanotube axis 2.8. The selection rules establish that the total angular momentum for electrons when absorbing a photon, the optical transitions from valence to conduction band must fulfill the rule;

$$\Delta m = \begin{cases} 0 & \text{for } \vec{E} \parallel z \\ \pm 1 & \text{for } \vec{E} \perp z \end{cases}$$

m is the total angular momentum quantum number and \vec{E} is the electric field. The previous condition shows the dependence of the relative polarization of the electric field vector to take a place the optical transitions. Thus, when \vec{E} is polarized in parallel direction to the nanotube axis (z -axis), m remains constant in the electronic band. On the other hand, if \vec{E} is polarized perpendicular to the nanotube axis, m changes the sign for plus or minus (depolarization effect) [29]. For SWCNTs we only consider the electric field polarized in parallel direction to the nanotube.

In addition, the optical transitions are symmetric respect to the valence and conduction band, i.e, the first energy peak in the valence band is related to the first

energy peak to the conduction band (E_{ii}^M or S). In such cases, the first optical transitions for metallic and semiconducting SWCNTs are given by

$$E_{11}^M(d_T) = \frac{6a_0\gamma_0}{d_T} \quad \text{For metallic nanotubes}$$

$$E_{11}^S(d_T) = \frac{2a_0\gamma_0}{d_T} \quad \text{For semiconducting nanotubes}$$
(2.13)

Consequently, the energy peak corresponds to the optical transition for electrons in the conduction or valence band. The **Kataura plot** shows the energy transitions related to the diameter of the SWCNTs, taking into account the resonance frequency between the photon and electron vibrations.

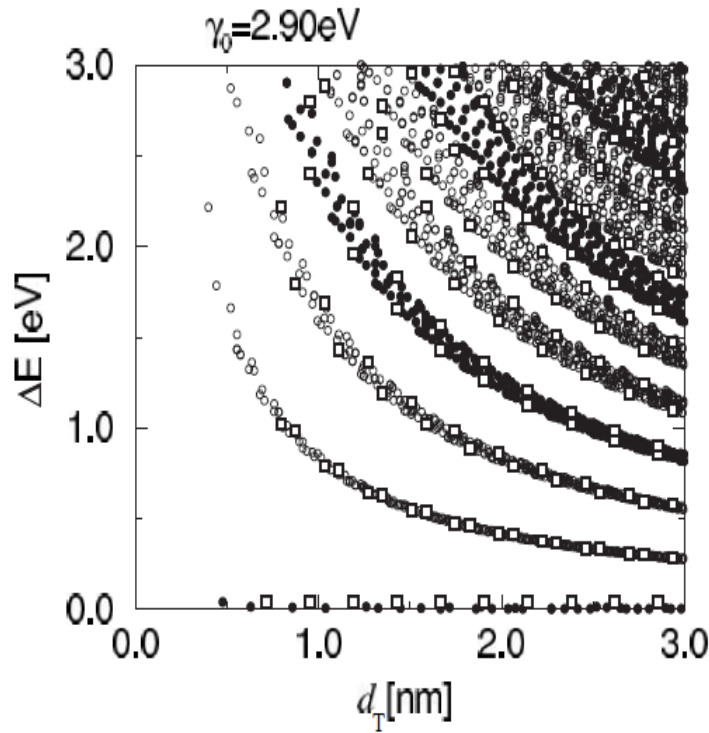


Figure 2.9: Energy separation for Kataura plot. For all values of chiral indices (n, m) as function of the nanotube diameter ($0.7 < d_T < 3nm$). The solid circles represent the metallic nanotubes whereas the dot circles represent semiconducting nanotubes. Along of the abscissa, the square dots represent the zero gap metallic nanotubes. Reproduced from Ref [7]

In Figure 2.9, the lines with open circles correspond to semiconducting tubes and the solid one to metallic tubes. The semiconducting character is seen by two

consecutive lines following the condition $n - m = 3l$ and the metallic character is seen by an intermediate line following the condition $n - m \neq 3l$. Noting that in the zero energy there are a lot of metallic nanotubes (along the abscissa axis), which is expected from the theory.

This remarkable result permits to explore the optical properties and electronic band structure of the SWCNTs by means of the optical responses. Their analysis carry out the resonance frequency that exhibits the electron energy transitions. Thus, when an electron absorbs a photon, its energy state changes from the valence to conduction band. It presents an energy transition which leaves a hole in valence and an electron in the conduction band.

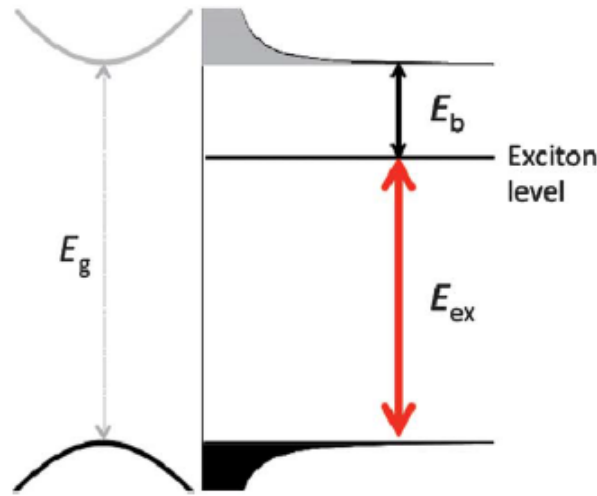


Figure 2.10: Scheme of electronic subband (E_{11}) (left) and density of states for exciton pairs (Right). E_g is the energy gap which provides information of the exciton energy E_{ex} and the binding energy E_b . Reproduced from Ref [7]

Such interaction is well-known electron-hole pair or exciton, Figure 2.10. On the other hand, the electronic resonances in different wave number ranges provides information regard to the amount of the nanotubes and their diameters. Both phenomena, exciton and electronic resonances for tube diameters are the optical responses to be analyzed in order to describe the electronic structure of SWCNTs and their optical properties and depending on the results, they can be used by different applications.

2.3 Substitutional doping

There are several functionalization paths that allow controlling the physical properties of carbon nanotubes. The extensive literature has not been unified regarding a classification of such methods. However, if we consider the outer and inner part

of the tube, as well as its wall, three type of categories can be defined: endohedral doping, exohedral doping and on-wall doping. The direct replacement of carbon atoms by heteroatoms falls in the on-wall doping category and I will not discuss this any further because it is an extensive topic that is not required for understanding the results obtained in this MsSc project. However, it is important to discern between the situations that arise from different doping levels with substitutional atoms. In other words, the properties of the substitutionally doped nanotubes can vary drastically depending on the number of heteroatoms that take the place of carbon. Leaving out the multi-walled nanotube case, two interesting concepts need to be described for a SWCNT: the high and low doping cases. In the next lines this is clarified. Additionally, for the specific case of boron, recent experiments in my hosting group have proved that ultra-low doping can have additional implications.

2.3.1 High doping and Low doping

Finding the boundaries between high and low doping is not a trivial matter. The necessity of a replacement of a large number of atoms can lead to the situation when the stoichiometry of the tube ends up in a repeating unit of C_xB_y configurations. In such situation we leave the doping concept and can start thinking about a tubular structure whose behaviour cannot be inferred from that of a pristine carbon nanotube. However, in the case of high doping, this should still be possible.

For the specific case of CB_x -SWCNTs the discussion regarding high doping levels is limited. The maximum replacement achieved by substitution reactions accounts for a 25%, where the generated stoichiometry is BC_3 . There are some experimental publications in this topic and additional theoretical works.

Regarding the low doping case, there is one concept that can allow identifying the above-mentioned threshold. That is the rigid band model, which is a concept widely applied in semiconductor physics. With this model, it is possible to estimate the properties of the doped material taking into account the pristine one with shifts of the van Hove singularities in reference to the Fermi level without changing radically the electronic structure as a whole. In this context, the threshold that defines when the rigid band model is not anymore applicable is the boundary between the high and low doping cases.

2.3.2 B-doped nanotubes: ultra-low doping

Although B-doped material with very low amounts of substitutional atoms have been reported, the applicability of the rigid band model has not been identified. The material that I have synthesized during this MsSc project seems to be an ideal candidate to achieve this task. The purification procedure developed within the group allows analyzing the nanotube material independently from the interference with catalytic byproducts. First doping estimations with x-ray photoelectron spectroscopy have given between 1 and 3 %at. However, preliminary results from the group have shown that ultra-low doping (in parts per mille) are necessary to keep the rigid band structure.

Chapter 3

Methods

This chapter summarizes the commonly used methods to synthesize pristine SWCNTs and the system used for this particular work to produce doped material. Additionally, the experimental methods to reveal and explore the optical properties for both pristine and doped SWCNTs are briefly explained. These are Raman, optical absorption (OA) and photoluminescence spectroscopies. These techniques allow analyzing the resonance frequency and emission-absorption spectra with different wavelengths or energy ranges in order to elucidate the diameter and chirality for pristine and doped SWCNTs.

3.1 Material Production Methods

After the SWCNTs discovery by Iijima in 1991, the nanotube scientific community has successfully optimized their production by three main methods: electric arc discharge, laser ablation and chemical vapor deposition (CVD) [9, 10]. In this work, I have used one adaptation of the last one, which is a high vacuum chemical vapor deposition (HV-CVD) system.

For growing SWCNTs, the use of a **catalyst** is required. The catalytic mechanism is different for each type of system because the temperature ranges at which the above mentioned methods work are completely different. This involves a completely different growth dynamics. In fact, the techniques for synthesizing SWCNTs differ in how the energy (temperature) required for breaking down the feedstock is generated.

For the particular case of CVD, growing SWCNTs requires a catalyst, usually composed of metals like iron (Fe), nickel (Ni), cobalt (Co) and others. These are not standard but some investigations have shed light into the reasons why one or other metal should work or not in specific systems.

In CVD, when the catalyst is put to high temperatures in presence of a feedstock, SWCNTs can grow from the catalyst, and parameters like temperature, pressure, chemical composition and other factors, can have a remarkable impact on the structural properties of pristine tubes, and even more in the case of doped tubes.

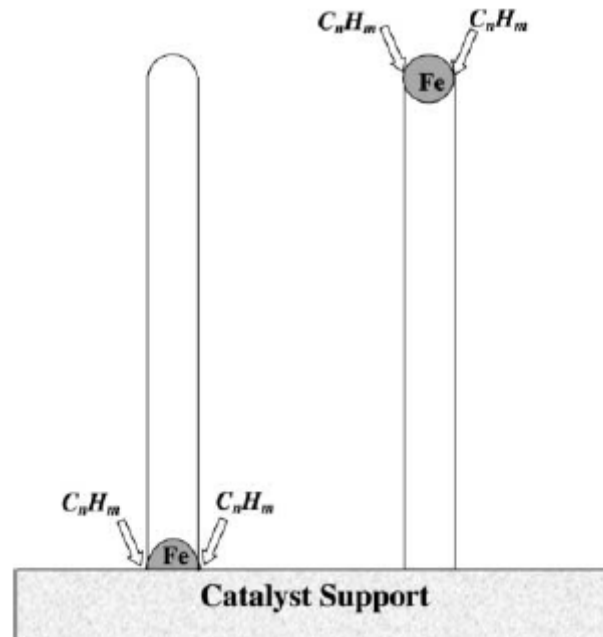


Figure 3.1: Scheme of SWCNTs growing around of Iron (Fe) catalyst. The CVD method exhibits two types of growing. Reproduced and modified from [10]

3.1.1 Electric Arc Discharge

This technique essentially consists of two electrodes of solid graphite, immersed in an inert medium like Helium or Argon gas in a chamber (Figure 3.2). The electrodes (cathode-anode) have a special feature; the anode is made of graphite with a metal catalyst like Fe, Co, Ni or Y, whereas the cathode is just graphite. When these electrodes site are close together and a high voltage generated between them, it produces an electric arc discharge similar to the welding, and as a consequence there is an evaporation of the electrode surfaces.

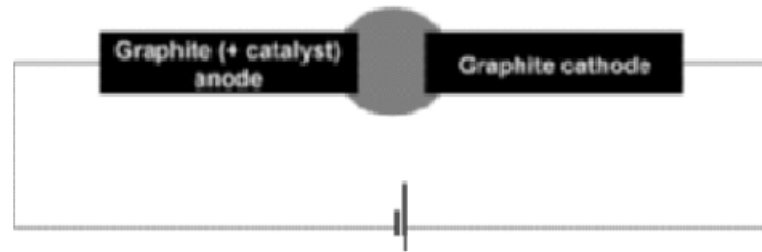


Figure 3.2: Schema of the electric arc discharge method. Reproduced from Ref [9]

The evaporating carbon changes its phase transforming from solid to gas (sublimating). The nominal temperature created by the electric discharge at the center is in the range of 2000 and 3000°C [9]. When the gas cools, carbon condenses back into a solid form. The resulting material is accumulated to a colder part of the chamber. It is possible to produce SWCNTs and/or in absence of metal catalysts, other type of carbon allotropes known as multi-walled carbon nanotube (MWCNT).

3.1.2 Laser ablation

This technique uses laser irradiation to vaporize the target. A graphite with metal catalysts located in a tube furnace. The furnace contributes to generating a gradient of temperature which influences the SWCNT or the formation of other carbon species. The temperature reached by the furnace is around 1200°C. An atmosphere of inert gas (it could be argon or helium) works as a carrier gas. At the end of the tube, there is a water-cooled collector (Figure. 3.3)

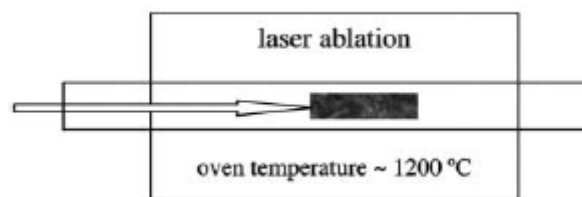


Figure 3.3: Scheme of Laser Ablation method. Reproduced from Ref [10]

The final product is a soot which can either be SWCNTs or MWCNTs depending of the experimental conditions.

3.1.3 Chemical vapor deposition

This technique involves high temperatures to heating of the catalyst in a tube furnace and the carbon feedstock is hydrocarbon gas which flows along of the tube for certain a period of time. The catalyst materials mostly reported are iron, niquel and cobalt (Figure 3.4).

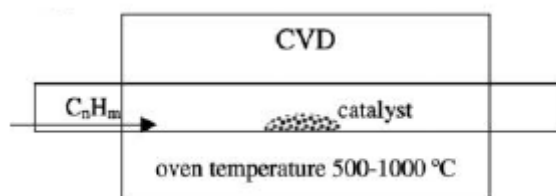


Figure 3.4: Scheme of chemical vapor deposition. Reproduced from Ref [10]

The nominal temperature for growing is about $550^\circ - 800^\circ$. The final product contains a great diversity of nanotubes (SWCNTs or MWCNTs).

3.1.4 High Vacuum Chemical Vapor Deposition

The experimental setup consists of a quartz tube in a furnace which produces a gradient of temperature along the furnace length, controlled by a voltage-current. The catalyst is inserted into to furnace. Then a high vacuum is generated by a turbo pump, controlled by the pressure gauge. When the catalyst reaches a high temperature, about $800^\circ - 1000^\circ$, a carbon feedstock containing also the desired substitutional atoms in a liquid state (C/B liquid stock) is evaporated into the furnace and it is pyrolyzed onto the catalysts.

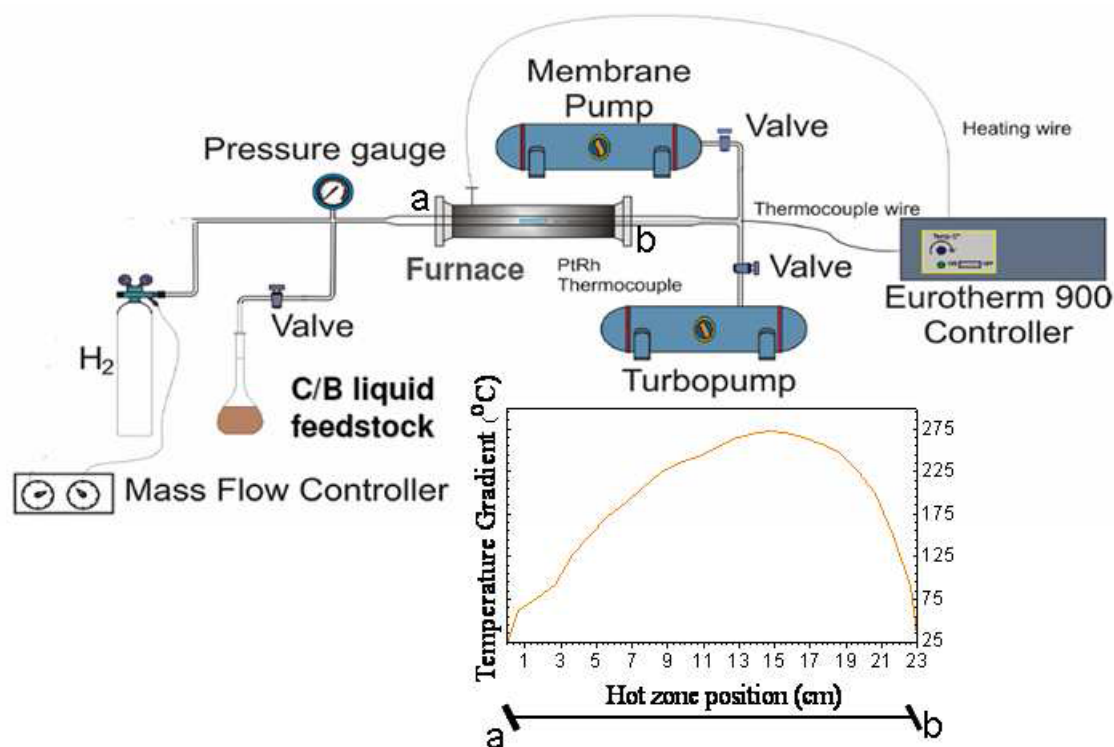


Figure 3.5: Scheme of High Vacuum - Chemical Vapor Deposition. Reproduced from Ref [3]

This leads to the formation of a tubular nanotube structure. The final product can contain diverse varieties of nanotubes (SWCNTs or MWCNTs) with different sizes, forms, and lengths depending of the carbon feedstock and external parameters.

The HV-CVD technique tends to produce SWCNTs cleaner or more controlled than other techniques being one of the advantages [2, 3, 10]. The control of external parameters like pressure and temperature allow the synthesis of (doped) SWCNTs to be controlled.

3.2 Optical Characterization methods

After growing SWCNTs (doped SWCNTs), the characterization of their properties provide information about which tubes are metallic or semiconducting. The usual method to characterize the properties in SWCNTs is the optical responses. Essentially, these responses are the resonance frequencies between electrons of carbon and photon that is exhibiting in energy transition. Thus, the diameter and chirality indices can be determined for SWCNTs (doped SWCNTs). The most used techniques are **Raman, optical absorption, and photoluminescence spectroscopies**. In this section, we will describe the mechanism for each spec-

troscopy technique to determine the features SWCNTs particularly, their optical properties.

3.2.1 Raman spectroscopy

The vibrational, rotational and low-frequency modes on matter can be analyzed by the Raman spectroscopy (RS). The RS technique employs a laser tuneable, which interacts with the sample and produce a *scattering* observed in the spectrum, i.e, the laser impinges with an electron cloud, changing its vibrational mode from ground to a virtual state. Then, the electron emits a photon and its final vibrational mode is different to its ground state.

If the virtual state of the electron is higher than the excited vibrational state, the electron emits a photon shifting in lower frequency in order to balance the total energy; this effect is called **Stokes shift**. If the virtual state is equal to the ground electronic state the effect is called **Rayleigh scattering**. If the excited vibrational state is lesser than the virtual state, the electron emits a photon shifting in higher frequency in order to balance the total energy; this effect is called **Anti-Stokes shift**. Those shifts refer to inelastic scattering where the final and initial energy states are not equal but the momentum is conserved (Figure 3.6a-c, respectively)

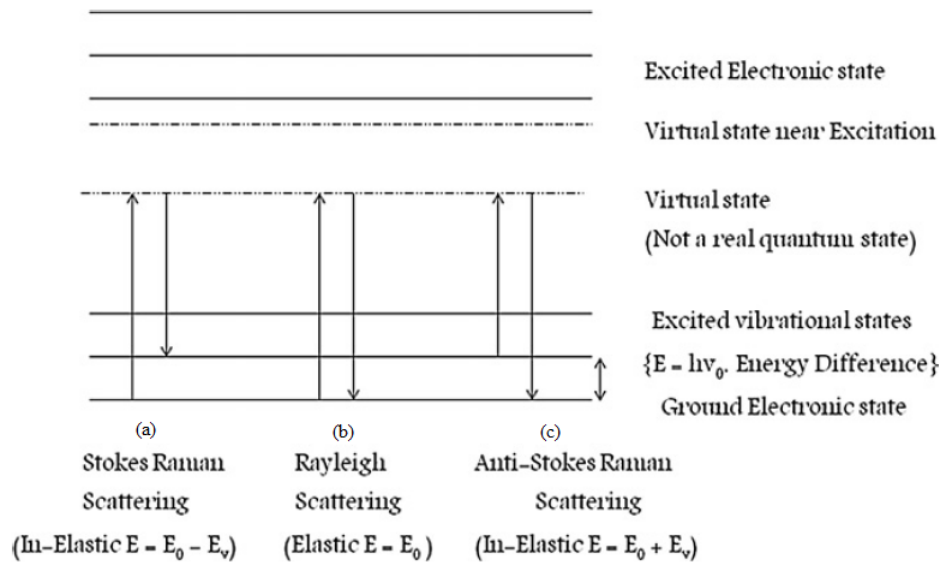


Figure 3.6: Raman scattering process. (a) Stokes shift, (b) Rayleigh scattering and (c) Anti-Stokes shift. Reproduced and modified from Ref [30]

These scattering processes carry out the total spectrum for SWCNTs (B-SWCNTs), which exhibit four main features. They provide information of the diameter in SWCNTs, defects on the crystal structure formed during the SWCNTs growing

and information of the substitutional dopants. The four main features are depicted as peaks (Figure 3.7)

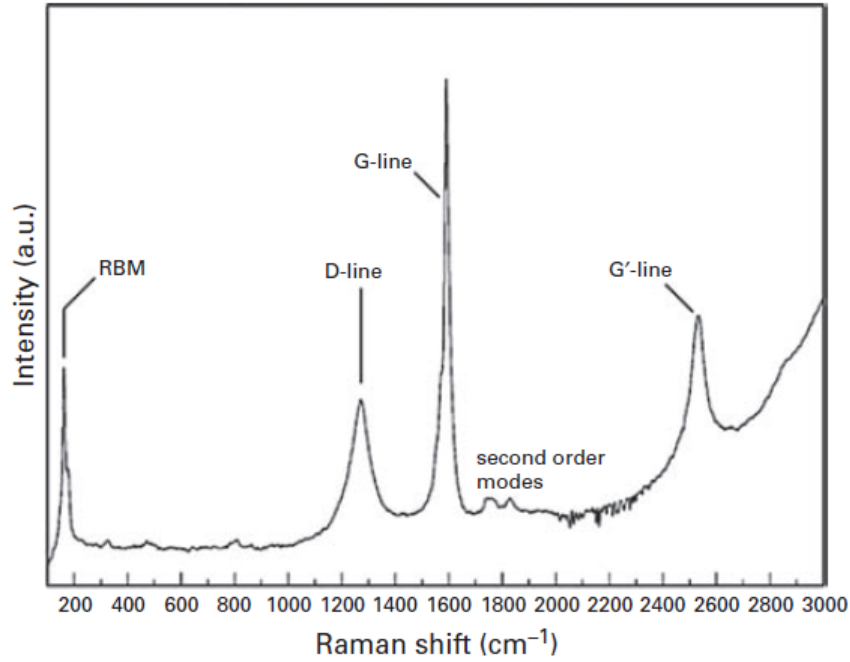


Figure 3.7: SWCNT spectrum by Raman spectroscopy. Reproduced from Ref [31]

In the Figure 3.7, the 4 main features in SWCNTs spectrum are classified as:

- Radial Breathing Mode (RBM): provides information of the nanotube diameter. The nanotube resonates in the range of $100 - 320\text{cm}^{-1}$. The RBM estimation for SWCNTs is an empirical relation [18]

$$\omega_{RMB} = \frac{234}{d_T} + 10 \quad (3.1)$$

where d_T is the diameter of the nanotube and the numbers are constants with length units [$\text{cm}^{-1} * \text{nm}$]

- The D mode: Provides information about the defects on the SWCNT structure or amorphous carbon; the peak is on the range of 1300cm^{-1}
- The G mode: Provides information about the tube is semiconducting or metallic and it usually is compared to RMB for the tube diameter estimation. The peak is in the range of $1580 - 1600\text{cm}^{-1}$
- The G' mode: Provides information to estimate roughly the nanotube diameter. The peak is in the range of $2500 - 2800\text{cm}^{-1}$

There are several types of Raman setups. Commercial instruments can be coupled to defined laser lines or to tuneable lasers. On the other hand, it is possible to use a tuneable laser that can allow the use of a larger number of frequencies. In addition, for my MsSc work, I have also used FT-Raman, which is a setup that uses a Fourier transformation from an interferogram to develop the spectral diagram. Because of the future work of my hosting group, it was particularly interesting to do FT-Raman analysis in the near-infrared (NIR) range, which is the spectral portion covered with this particular technique. The SWCNTs exhibit high peaks because the carbon electrons resonate more in this range. Part of the applications for SWCNTs are envisaged for biologic systems, whose tissues are actually transparent in NIR range [32].

3.2.2 Optical absorption spectroscopy

The energy transitions of an electron in an excited state, leaves a hole on the electronic band structure and the electron-hole pair created is well-known as exciton (Figure 2.10). In SWCNTs, the energy transitions have particular differences regard to the semiconducting and metallic character in the nanotubes. Thus, the electronic density of states (DOS) exhibit energy transitions longer in metallic than semiconducting nanotubes 3.8

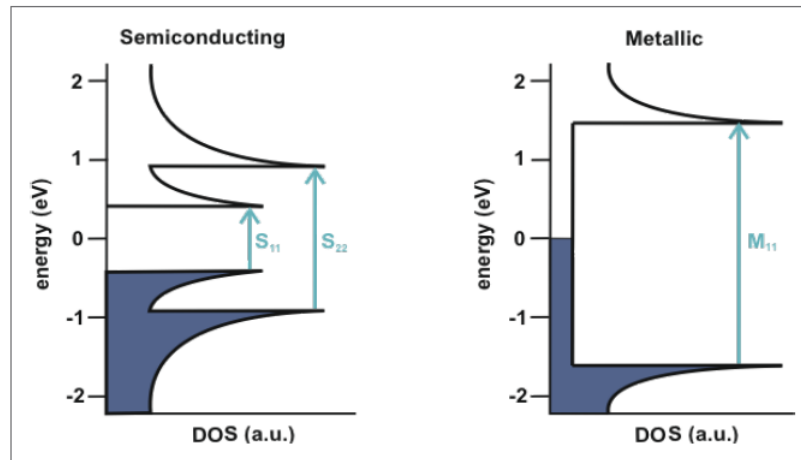


Figure 3.8: The optical transitions in SWCNTs. In semiconducting tubes the transition S_{ii} is smaller than in metallic M_{ii} tubes. Such feature is measured by optical absorption spectroscopy collective oscillation of the π -electron density. Reproduced from [33]

The vHs represent how the electrons in valence band change their energy and occupy the conduction band. Thus, the optical absorption spectroscopy are an useful tool which provides the information about the energy transitions in SWCNTs.

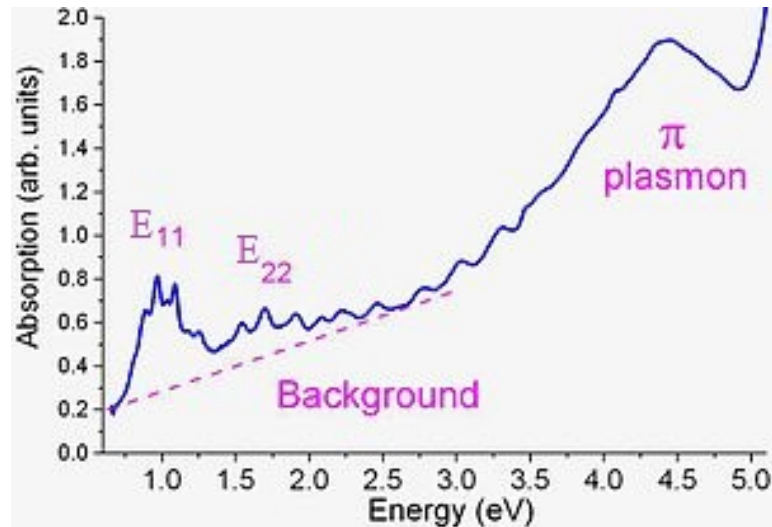


Figure 3.9: The optical absorption depending on the photoemission and the absorption. The peaks correspond to first and second energy transitions E_{ii} . The last one peak is the π – *plasmon* energy or the collective oscillation of the π -electron density. Reproduced from [34]

Each energy peak produced by the optical absorption spectra is related to the diameter of the nanotube and chiral indices because the exciton transitions indicate the resonance energy with the light showing a peak into the spectrum. It verifies the spectrum in the visible and infrared range. Kataura et al [35] showed the relation of the optical absorption regard to the diameter distribution in SWCNTs and currently it is used like a map to derive the metallic and semiconducting character of SWCNTs.

3.2.3 Photoluminescence spectroscopy

The optical responses of the SWCNTs (doped SWCNTs) lie on the selection rules for conservation of total angular momentum which gives information about their electronic structure. Such responses are produced by the exciton interactions and they strongly depend of the light polarization.

The exciton interaction is owing to the optical transition of electron-hole bond, wherein an electron absorbs a photon (particularly parallel-polarized along of the nanotube) left a hole on the band energy; afterwards, the electron emits a photon with different energy and recombining with the hole (Figure 3.10).

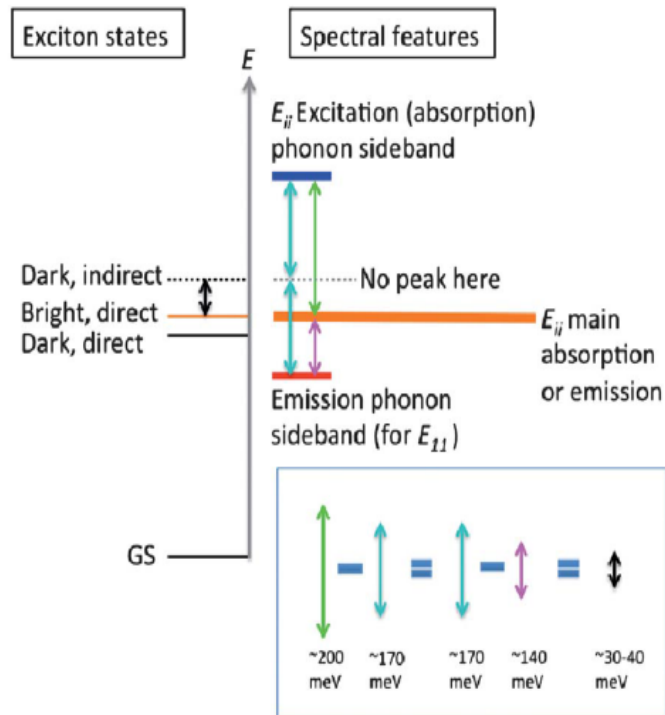


Figure 3.10: The optical excitations process. (Right) It corresponds the energy exciton levels, and (Left) the energy peaks produced by PL or absorption. Reproduced from [7]

The photoluminescence (PL) spectroscopy analyses the optical transitions of electron-hole pair, according that each energy peak is produced by a resonance fluorescence. As consequence of those peaks, the chiral indices are assigned for semiconducting and metallic nanotubes (Figure 3.11).

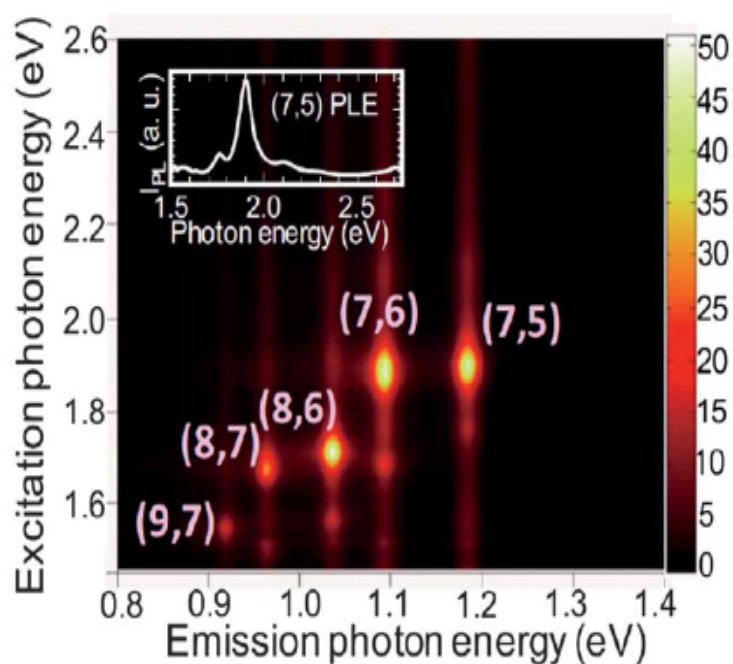


Figure 3.11: The optical excitations in PL spectroscopy. The brightest points indicate the maxima energy excitation which can be plotted as a peak. Reproduced from [7]

The PL spectroscopy for SWCNTs has allowed to design a map that illustrates the emission in photon energy versus excitation photon energy for each chiral indices and diameter. This map is called **PL map**; noting that PL map is related by the Kataura plot (Fig 2.9). Each photo-emission vs excitation photon energy value relates the nanotube diameter according with [35].

Chapter 4

Production of CB_x-SWNTs

The growth of CB_x-SWNTs implies a long process of production if one aims at having a good quality material that allows characterizing their properties. For pristine carbon nanotubes it is believed that the selection of catalyst determines the nanotube diameters in a sample. However, this does not seem to be the case for B-doped nanotubes and it still has to be understood. After the growth of CB_x-SWNTs, the catalyst material and amorphous carbon must be removed of CB_x-SWNTs. When the sample is purified, it is possible to study its electronic and optical properties. In this chapter, we briefly overview the process carried out to produce and purify CB_x-SWNTs.

4.1 Growing process of CB_x-SWNTs

For CB_x-SWNTs synthesis, we employed a catalyst material composed by iron nitrate (Fe(NO₃)₃) and magnesium oxide (MgO). The concentration for both catalyst materials were changed according with the spectrum analysis after the CB_x-SWNTs growing by means of raman and FT-raman spectroscopy. We tested 4 different concentrations of catalyst in percentage orders summarized in the Table 4.1

To mix the catalyst, we employed isopropanol methanol (CH₃OH) (20 milliliter). For optimizing the mixture dissolution, a sonication device allows such process, and about 5 hours, the mixture can be used for synthesis.

Concentration %	
Iron nitrate	Magnesium oxide
15	85
20	80
25	75
30	70

Table 4.1: Catalyst concentration for CBx-SWNTs growing. The total weight for the concentration is 1250gr

Nevertheless, the mixture in the liquid phase state is extremely volatile for methanol content. Hence, it was drying in a small oven at 50°C . After the drying, the mixture was weighted and collected in boots devices for the synthesis.

The experimental technique for CBx-SWNTs synthesis was HV-CVD (see Figure 3.5). The high vacuum favoured the reduction of oxygen around of the catalyst or another impurities. The turbo pump vacuum could reached about $10^{-6} - 10^{-8}$ millibar, necessary condition to synthesize SWCNTs. After the high vacuum, a voltage controller allows to reach the temperature for break down the carbon feedstock.

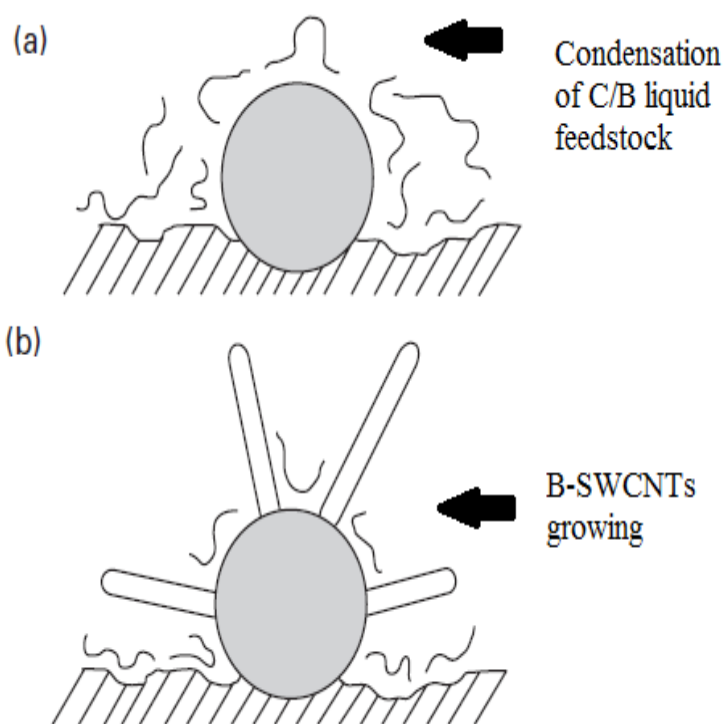


Figure 4.1: Schema of SWCNTs growing extended to CBx-SWNTs. (a) The C/B liquid feedstock passes through the furnace and it condensates to deposits in the surface of catalyst. (b) Nanotube growing. Reproduced from [12]

With the proper temperature and pressure conditions for the synthesis, the turbo

pump was closed and the synthesis of CBx-SWNTs at 800°C with 10^{-6} millibar was achieved. The carbon feedstock selected for the synthesis was Triisopropylborate ($[(\text{CH}_3)_2\text{CHO}]_3\text{B}$). The C/B liquid feedstock pyrolyzes when it passes through of the heat zone of the furnace and together with the catalyst forms the nanotubes (Figure 4.1a). One of the growth models can be seen in Fig. 4.1b.

After the CBx-SWNTs growing, the final product contains a set of long nanotubes with different diameters called *bundles*. Around of the nanotubes are attached several amorphous carbon like fullerenes and others, then, it is necessary to separate them from the SWCNTs (purification process). In order to verify if the bundles contain SWCNTs, we used the raman and FT raman spectroscopy. Firstly, the raman spectroscopy with a laser of 633nm exhibited the *RMB*, *D*, *G* and *G'* lines expected. For each catalyst concentration we found SWCNTs (Figure 4.2).

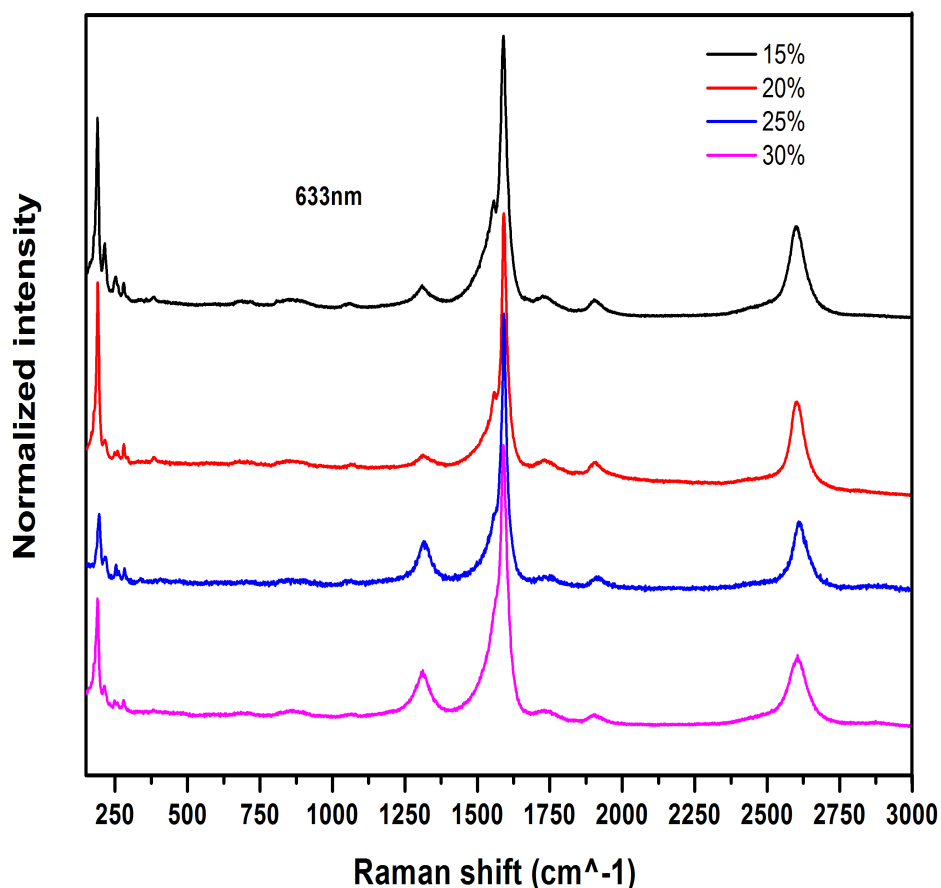


Figure 4.2: Spectrum of SWCNTs after the synthesis (Not purified) extended to CBx-SWNTs. Each color corresponds to the catalyst concentration with data were normalized in terms of the intensity.

In the previous spectrum, we found that the catalyst concentration of 25% has an intensity well-defined in G-line respect to the others. G-line confirms that the substitutional heteroatoms boron is in the SWCNT, thus we proceed to produce more CBx-SWNTs with this concentration. Remarkably, each catalyst concentration in *RMB*-line band, exhibits different diameters (Table 4.2). The diameter can be determined with the equation 3.1

Concentration (%)	ω_{RMB} (100-300 cm^{-1})	Tube diameter (nm)
15	132.29	1.91
	189.58	1.30
	214.58	1.14
	252.08	0.96
20	132.29	1.91
	190.65	1.29
	215.62	1.13
	248.95	0.97
25	258.20	0.94
	105	2.4
	123.95	2.07
	131.25	1.93
	212.5	1.30
30	279.16	1.26
	194.79	1.12
	218.75	0.96
	253.125	0.85

Table 4.2: Approximated diameters in RMB-line (100-300 cm^{-1}). The spectrum was analyzed with a laser in the range of 633nm for CBx-SWNTs without purification process.

4.2 Purification process

The pristine sample contains an important amount of impurities like amorphous carbon. To separate them from the bundle, it usually employs a chemical compounds to remove the catalyst materials and mechanical process to select nanotubes with low density of carbon allotropes.

Firstly, the chemical compound used for the CBx-SWNTs purification is hydrochloric acid. It removes the metal elements in the pristine. The sample sites on the top of an Erlenmeyer flask with a filter paper and a funnel holds the paper in order to pour the acid on the sample. During 3 hours, the sample is cleaned with distilled water. The final product brings out in low temperatures to evaporate the oxygen.

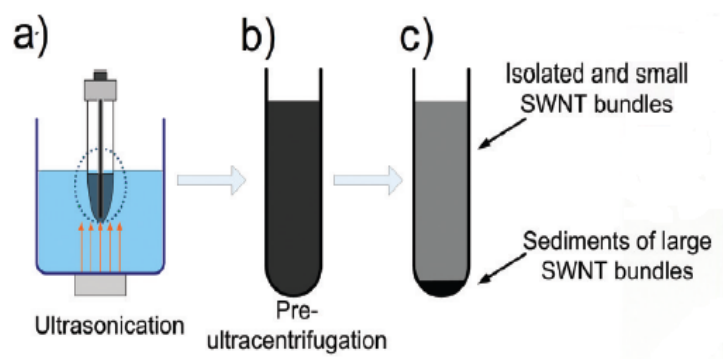


Figure 4.3: Schema of the purification process from ultra-sonication to ultracentrifugation (a-c). Reproduced and modified from [36]

Secondly, the result material contains an undetermined amount of amorphous carbon in the bundles. If it analyzes the sample in this stage, several electrons from the amorphous carbon could resonate in unexpected frequencies when the sample is analyzed in photoluminescence and optical absorption spectroscopy. In order to obtain purify samples, the density gradient ultracentrifugation separates in different density levels the SWCNTs bundles [36]. Essentially, the sample partially purified without metal catalyst, can bring under ultra-sonication devices. The sample mixes with a chemical compound which creates bubbles that holds the CBx-SWNTs bundles dispersed. We employed deoxy cholate sodium salt (DOS) to mix the sample without metal catalyst by ultra-sonication about 5 hours (Figure 4.3a).

Afterwards, using an ultracentrifugation devices, it separates in different gradients the CBx-SWNTs bundles. The exposition time for ultracentrifugation is 30 minutes (Figure 4.3b-c). With this techniques, we proceed to determine the chiral indices (n, m) for CBx-SWNTs and its corresponding metallic and semiconducting character using optical absorption and photoluminescence spectroscopy.

Chapter 5

Optical Characterization of CB_x-SWNTs

To characterize the optical responses of CB_x-SWNTs, we focused in both purified and non-purified samples with different iron nitrate concentration in the catalyst. Firstly, we use the raman and FT-raman spectroscopy as initial stage to determine if our samples contain SWCNTs comparing their spectrum accordingly with fig. 3.7 looking at the shape of the G' band and the radial breathing mode (RBM).

Secondly, we used the optical absorption spectroscopy for such samples to determine more accurate their tube diameters and chiral indices according to their energy transitions in E_{11} (1000-1500nm) and E_{22} (500-1000nm). Finally, we used the photoluminescence spectroscopy to better approximate if the chirality obtained are present in both samples.

5.1 Raman spectroscopy results

The non-purified and purified samples were analyzed with different laser lines at 458, 514, 568 and 633nm, respectively (Figure 5.1). At 458nm-514nm, the RBM has narrow peaks and low intensities, whereas at 568nm-633nm, the RBM has high intensity. Altogether samples exhibited high intensities in G-mode, low intensities in D and G'-modes.

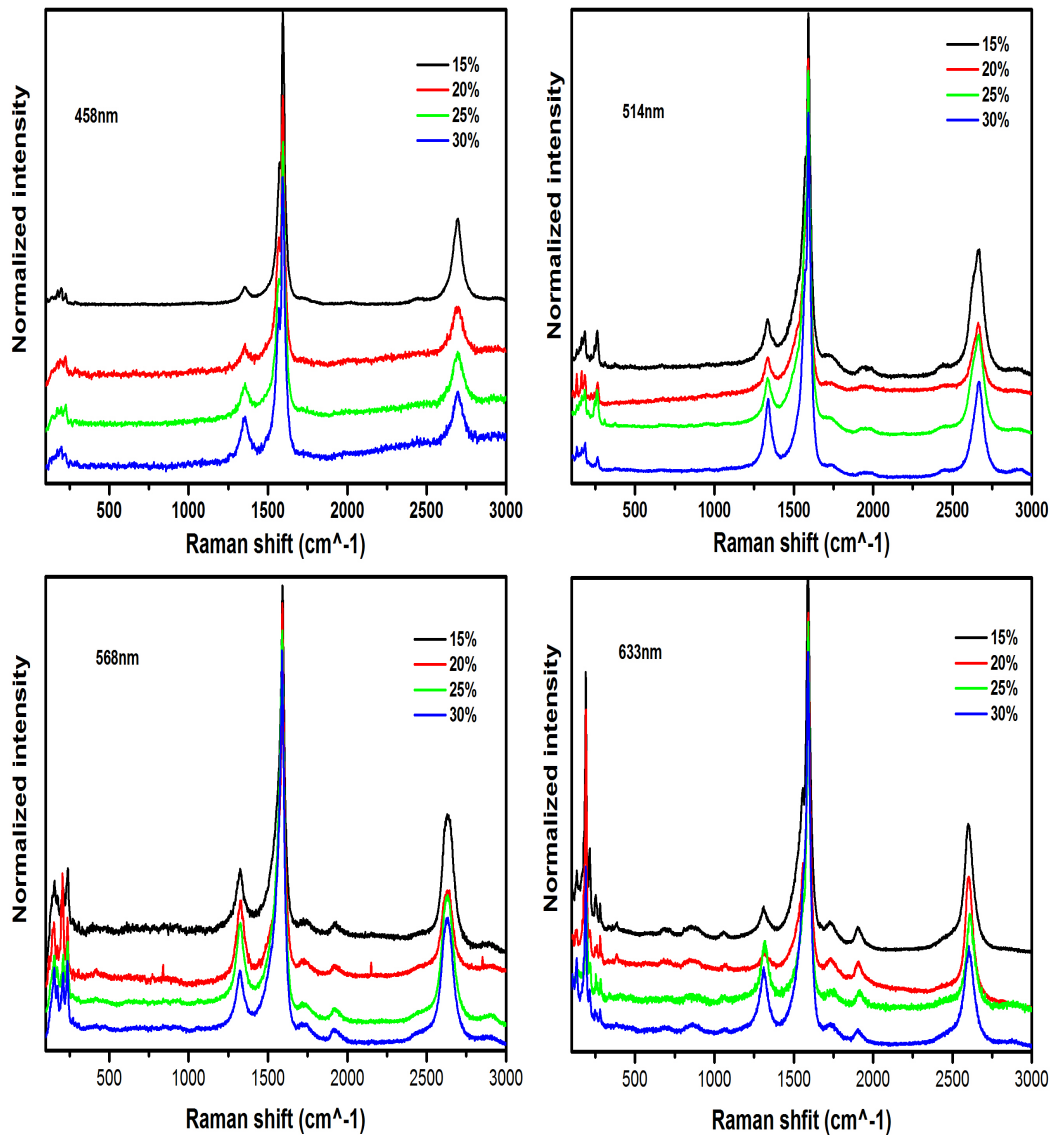


Figure 5.1: Raman spectroscopy for non-purified CB_x-SWCNT. The color lines correspond to the iron nitrate concentration (%). The laser lines employed at 458, 514, 568 and 633 nm. The peaks exhibited for each sample, vibrate into the SWCNTs range.

From that plot, we confirmed that the spectrum for each non-purified samples exhibit vibrational modes into the range of SWCNTs modes. So, the RBM, D, G, and G'-modes were obtained and compared with the plot in Fig.3.7. Focusing our attention in the tube diameter in the samples, we proceeded to analyzed the RBM ($100 - 350 \text{ cm}^{-1}$). We used different laser lines because if it uses only one of them, it cannot provide information in different regions of RBM, i.e, the lasers excite electrons of our samples in different regions of RBM and they contribute to determine the diameter distribution of the nanotube.

The plots in Fig. 5.2(a-d) correspond explicitly to the RBM region and reveals

the peaks for each sample and laser line. Each peak has particular values in the Raman shift-axis with its corresponding value of intensity. Additionally, each peak corresponds to the response of one type of tube specifically. Using the eq.2.4, we could roughly determine the diameter of the tube, which is indicated on the top axis in the plot. We observed a great variety of diameter in the tubes, which demands to perform a curve fitting for each spectrum and sample to determine more accurate the diameter distribution of the tubes.

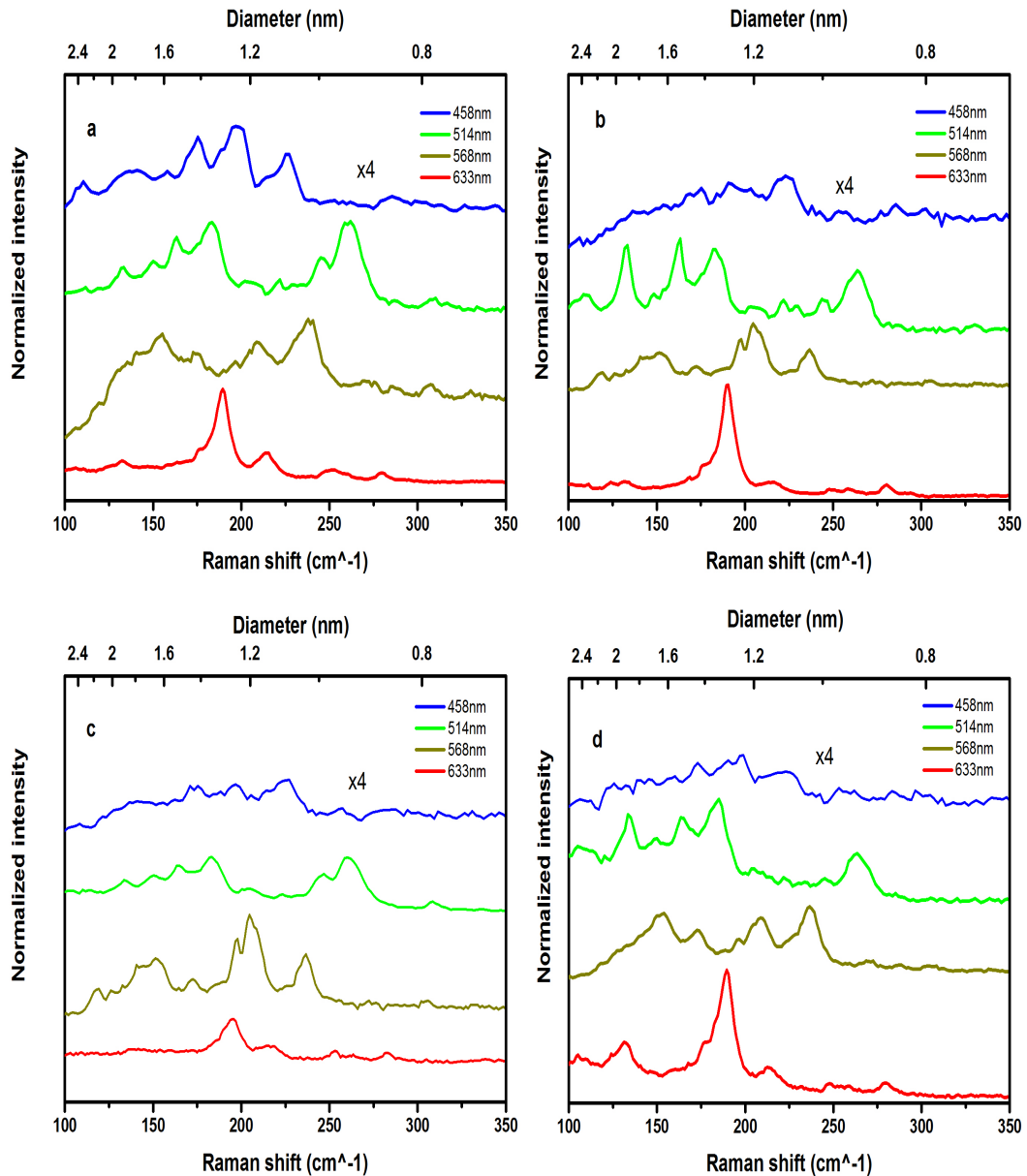


Figure 5.2: RBM range for determination of tube's diameter. The color lines correspond to laser excitation. From a to c refer to the samples 15, 20, 25 and 30% iron nitrate concentration, respectively.

We individually fitted each spectrum according with its peaks excitation by means of **Voigt fitting**. We found the intensities and the diameter associated for each

peak excitation. Thus, we took the peaks below to the original spectrum, the diameters and intensities were registered for each sample with each laser line, e.g, the sample with 15% of iron nitrate concentration non-purified, as depicted in fig.5.3

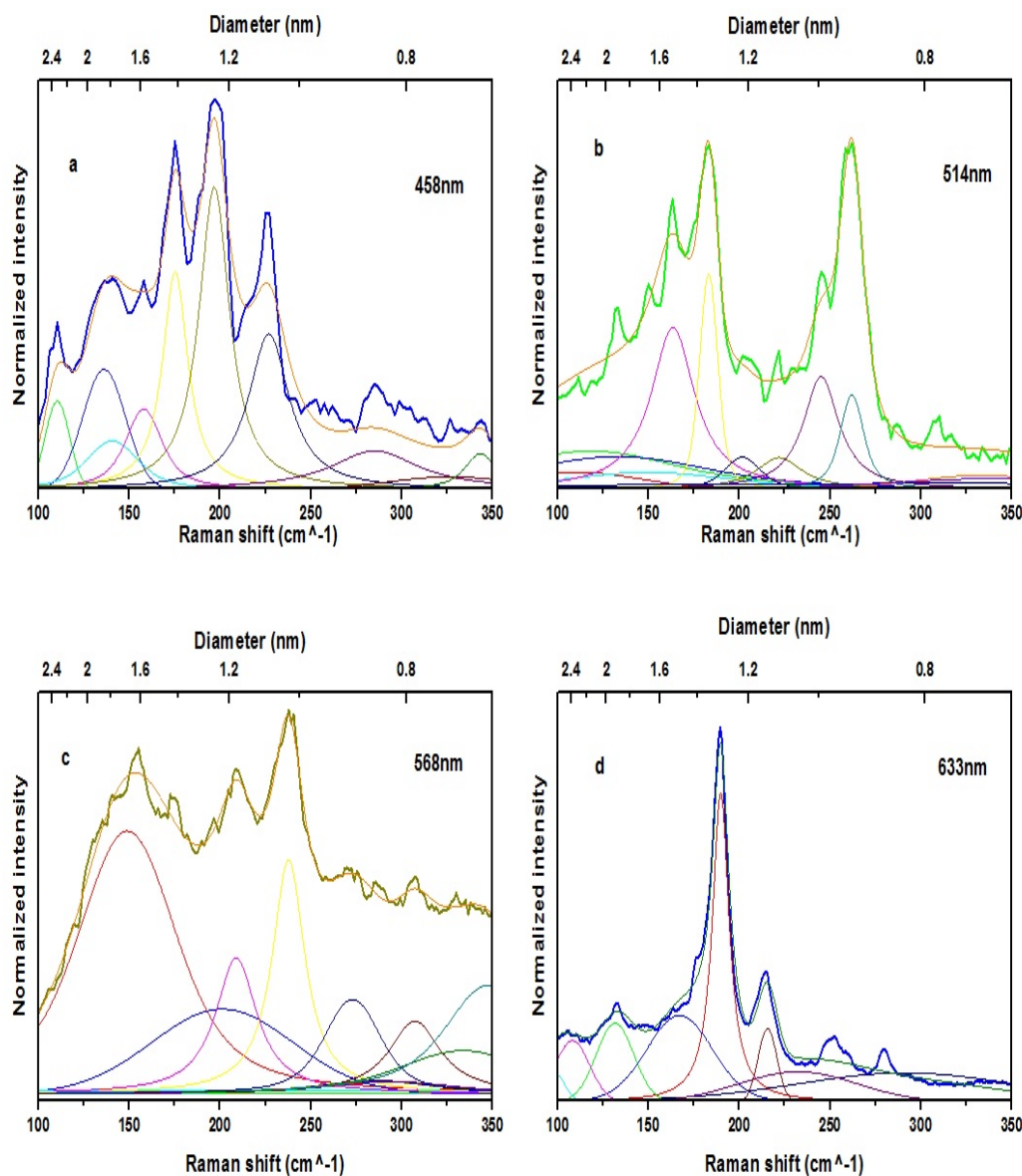


Figure 5.3: Voigt fitting for determination of tube's diameter for sample at 15% of iron nitrate concentration. The color lines correspond to laser excitation (a to d) for the sample 15% of iron nitrate. This procedure extends to the other samples.

As result of the previous fitting, we collected such information and plotted them in column plots in order to determine the diameter distribution of the tube for all non-purified samples regard to the laser line excitation. The diameter distribution was estimated by fitting with **the extreme statistic fitting** (Fig.5.5). Each non-purified sample contains different tube's diameter distribution in which case

their values are close. In spite of the tube's diameter are not significantly high between each other, we considered to compare the tube's diameter from purified sample and compare it with the non-purified sample. We selected the 25% of iron nitrate concentration sample to purified because that one exhibited remarkably high peaks in G-mode and it has well-defined peaks in RBM-mode with different laser excitation (see Fig.5.1).

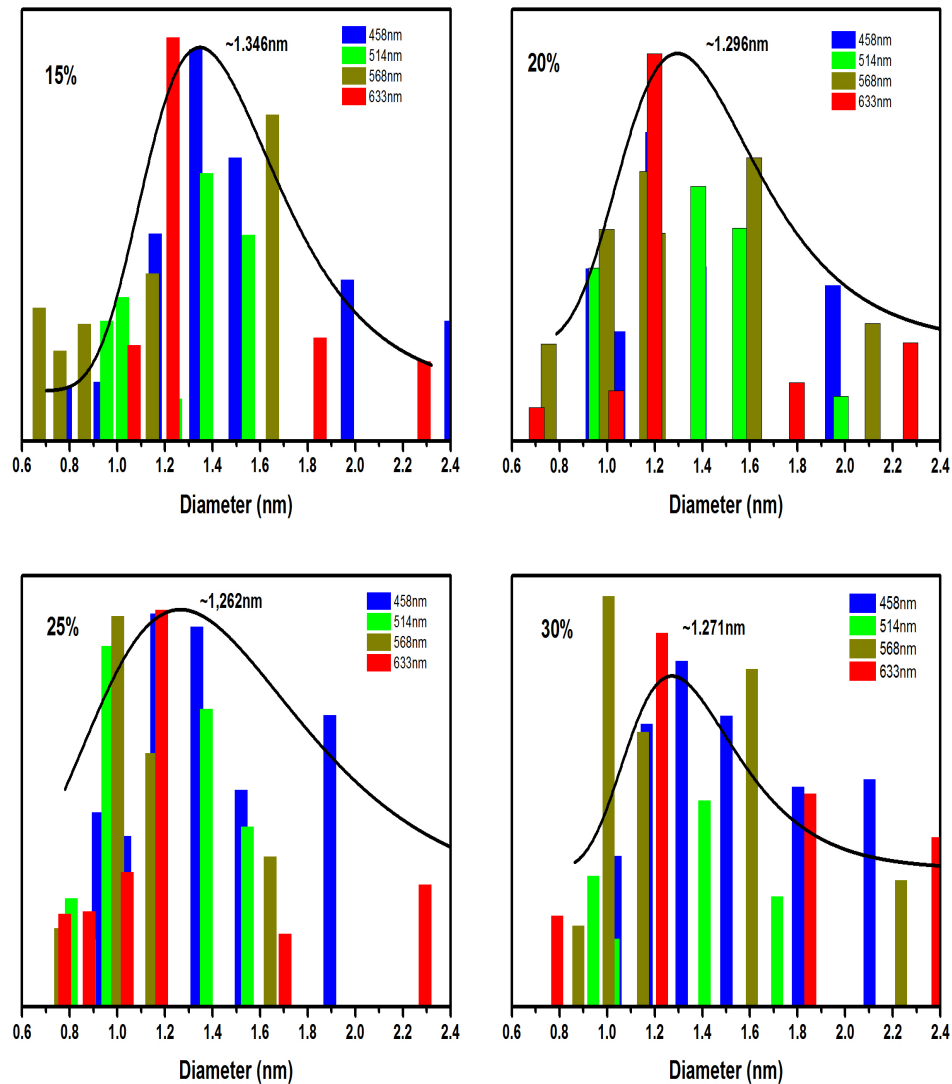


Figure 5.4: Diameter distribution of the observed tubes for all non-purified samples. The color bars correspond to peak intensity produced in the RBM region according to the laser excitation. The fitting technique employed was the extreme statistic fitting. The 15% sample has a diameter of 1.346 nm, 20% has 1.296 nm, 25% has 1.262 nm and 30% has 1.271 nm

To determine the diameter distribution for purified sample at 25% of iron concen-

tration, we employed the same procedure but we just used the laser line at 633 nm. We found that both samples have a diameter distribution of 1.287 nm. We cannot say if the diameter change under the purification process. In fact, the purification process can be responsible for the destruction of certain nanotube species with specific diameters. Usually, nanotubes with smaller diameters are lost after purification. We observed the purified sample resonates almost in the same range of non-purified sample with the same iron nitrate concentration in the catalyst.

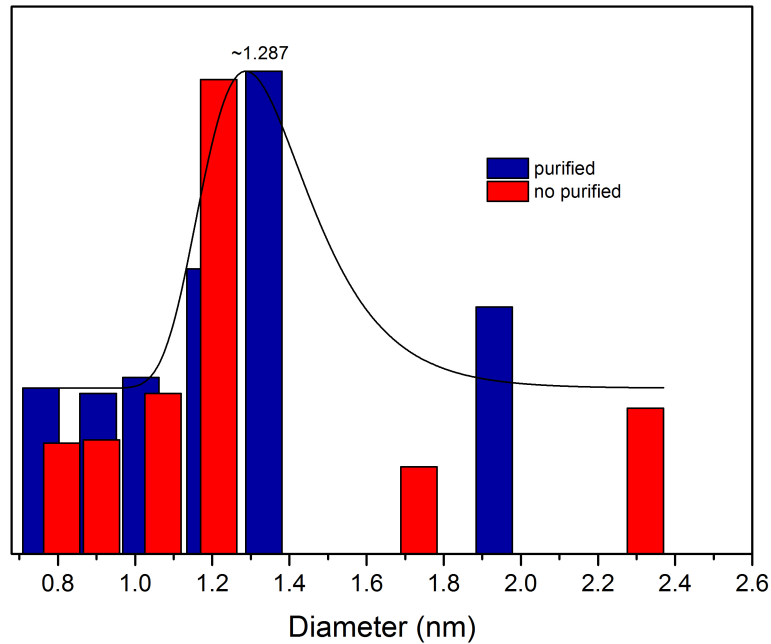


Figure 5.5: Comparison of the diameter distribution for purified and non-purified samples at 25% of concentration. This graph shows the data corresponding to the spectra recorded with the laser line at 633 nm. The color bars correspond to the peak intensities produced in the RBM region and the diameter distribution is centered 1.287 nm. The convoluting approximation was done with an fitting technique employed was the extreme statistic fitting.

With Raman spectroscopy we were able to verify that our samples contain SWCNTs. In principle, the doping effect by Boron can also be investigated with this technique, however this is not the matter of discussion of this master thesis. This would involve a detailed study of 2D-band. Finally, it is necessary to recall that the D-mode provides information about the defects into the tubular structure of the nanotube due to amorphous carbon or dopants into the lattice of a SWCNT, but we cannot draw conclusions in this respect from our spectra. All samples have similar spectra and we only observed different tube diameters in the RBM.

5.2 FT-Raman spectroscopy results

The same non-purified and purified samples were analyzed into the range of near-infrared (800-2500 nm) (figure ??). The RBM has narrow peaks and high intensities. In G and D' modes, all samples exhibited high intensities. The background produced in the range of 2000-2500 cm^{-1} is owing to counts per cycle for collecting data.

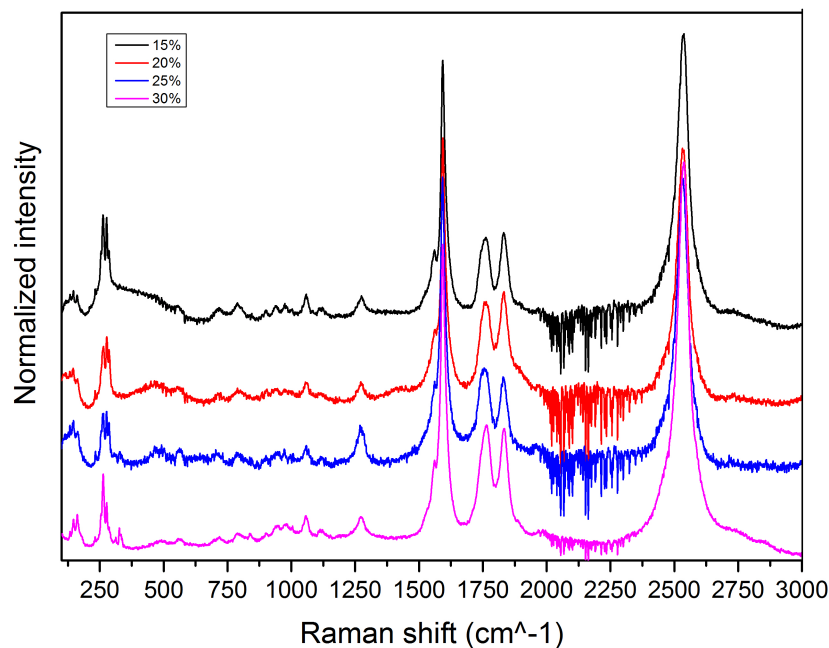


Figure 5.6: FT-Raman spectroscopy for non-purified B-SWCNTs. The color lines correspond to the iron nitrate concentration (%). The peaks exhibited for each sample, vibrate into the SWCNTs range.

To determine the tube diameter distribution, we used the same procedure of Raman spectroscopy, i.e the selection of the peak intensities for fitting.

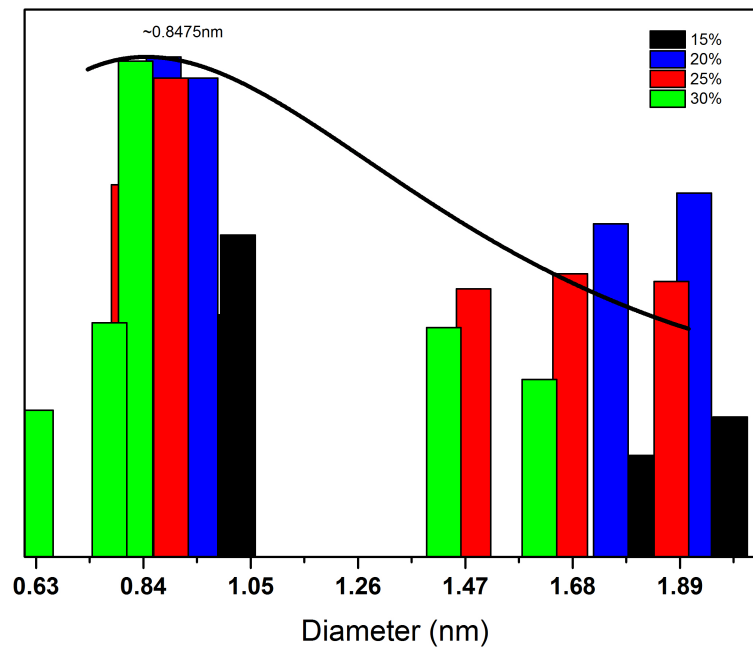


Figure 5.7: The diameter distribution for non-purified samples at 15, 20, 25, 30% of iron nitrate concentration. The color bars correspond to concentration of iron nitrate. The fitting line shows an approximated diameter of 0.847nm

I have done the analysis of FT-Raman independently because it is useful for further applications. SWCNTs have very strong optical response in the region where the biological tissues are transparent. Therefore having a record of the Raman response in the infrared region is particularly important.

5.3 Optical absorption spectroscopy results

We employed the non-purified and purified samples with 25% of iron concentration for this technique. The optical absorption spectroscopy uses the all spectrum range of light to explore the energy transitions when the electrons pass from valence to conduction band. Such energy transitions allows to determine the diameter of the nanotube and its chiral indices. For non-purified sample, we observed three small peaks in the range of E_{11} and E_{22} energy transition, while the purified sample, we just observed two small peaks in the same energy range. Table 5.1 summarizes the obtained data:

Non-purified sample				
$E_{22}(eV)$	$E_{11}(eV)$	Diameter (nm)	Chiral indices	Feature
2.0001	1.184	0.822	(7,5)	semiconducting
1.95	1.085	0.866	(7,6)	semiconducting
1.97	1.264	0.777	(8,3)	semiconducting
Purified sample				
$E_{22}(eV)$	$E_{11}(eV)$	Diameter (nm)	Chiral indices	Feature
2.246	1.254	0.752	(6,5)	semiconducting
2.109	1.111	0.833	(8,4)	semiconducting

Table 5.1: Energy transitions for non-purified and purified samples at 25% of iron concentration. The chiral indices for both samples point out semiconducting features in the nanotubes.

According to Fig. 2.9, the Katuara plot relates the energy with the tube's diameter. Thus, we related the energy peaks observed in regard to the diameter of the nanotube and their correspond chiral indices [37]. Notably, both samples exhibited different energy transitions due to the purification process in one of the samples. The non-purified sample contains a high population of three types of nanotubes with different diameters, whereas the purified sample contains just two.

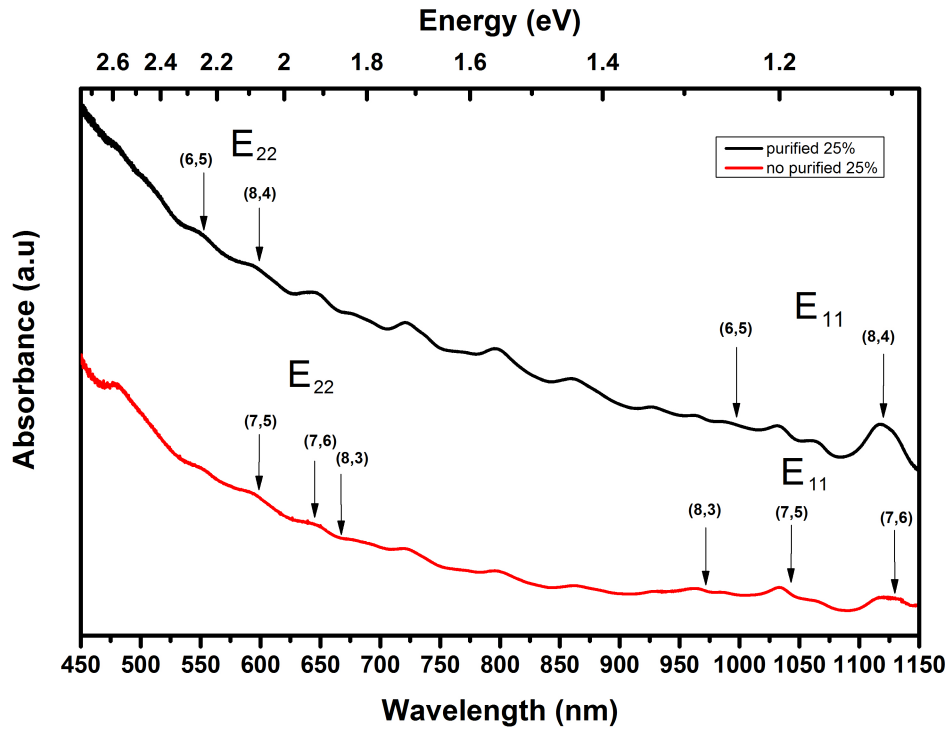


Figure 5.8: Optical absorption spectroscopy for non-purified and purified B-SWCNTs. The E_{11} and E_{22} correspond to the energy transition for both samples. The brackets correspond to chiral indices associated for each diameter

Comparing the diameter distribution observed in Raman spectroscopy with the diameter observed in the optical absorption spectroscopy, the diameter observed in optical absorption is the range of 0.7-0.8 nm while in Raman is 1 nm range. Such result owing to the purification process explicitly implies the separation of amorphous carbon in a suspension and the resultant sample is not bundle in which case its detection is really challenging. For that, optical absorption spectroscopy is a complementary technique that yields to compare the diameter obtained in the samples.

5.4 Photoluminescence spectroscopy

Using the same non-purified and purified samples, we measured the samples in the range of 570-598 nm which corresponds a small range of E_{22} energy transition. For non-purified samples, we plotted the emission vs excitation wavelengths and we observed nanotubes with (6,5) and (8,4) of chiral indices (Fig.5.9). Each one has a diameter of 0.752 nm and 0.8335 nm, respectively.

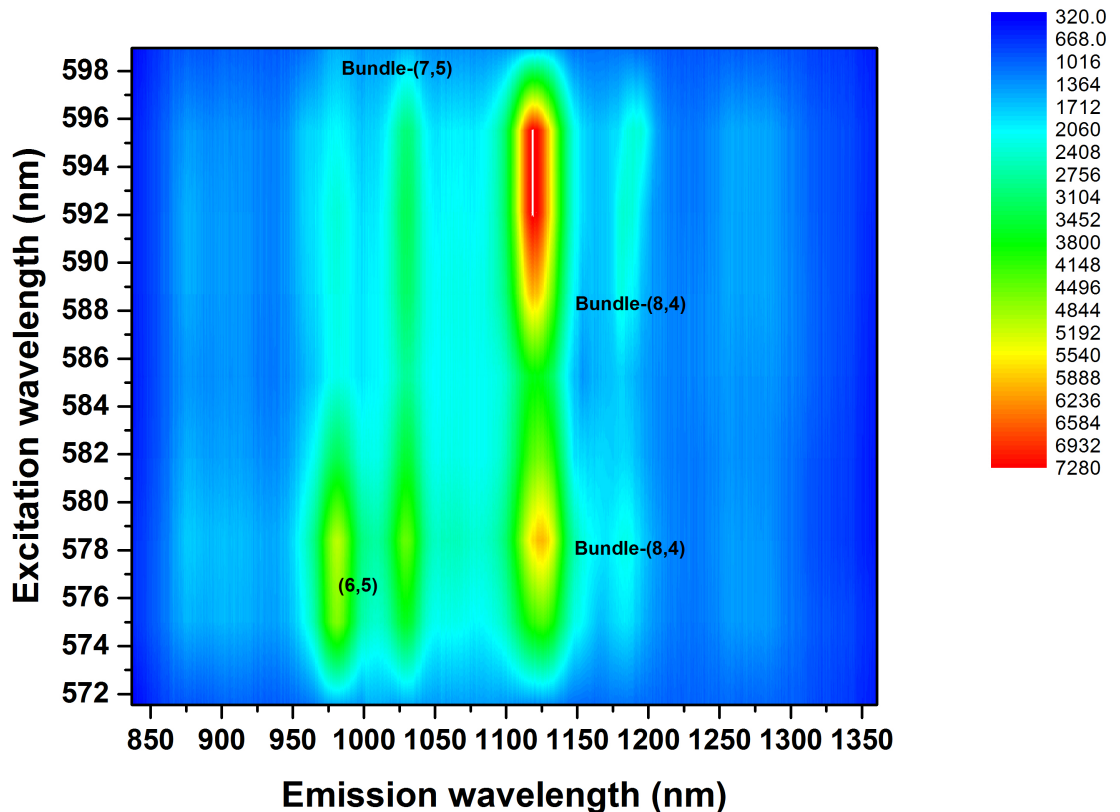


Figure 5.9: Photoluminescence spectroscopy for non-purified sample. The chiral indices assigned are different from the chiral indices assigned in optical absorption.

For a (6,5) tube, the energy transitions are E_{11} with 2.187 eV and E_{22} with 1.272 eV. Equally for (8,4), the energy transitions are E_{11} with 1.114 eV and E_{22} with 2.112 eV. Both assigned chiral indices differs to the assigned indices from optical absorption.

On the other hand, it was extremely difficult to study the purified sample, which did not exhibit any emission and excitation localized wavelength in order to assign the corresponding chiral indices and therefore, their diameter and character cannot be assigned (Fig.5.10). Due to the processes which occurs during the recombination process between electrons and holes, the photon relaxation or fluorescence re-emission has low energy that complicates the measurements

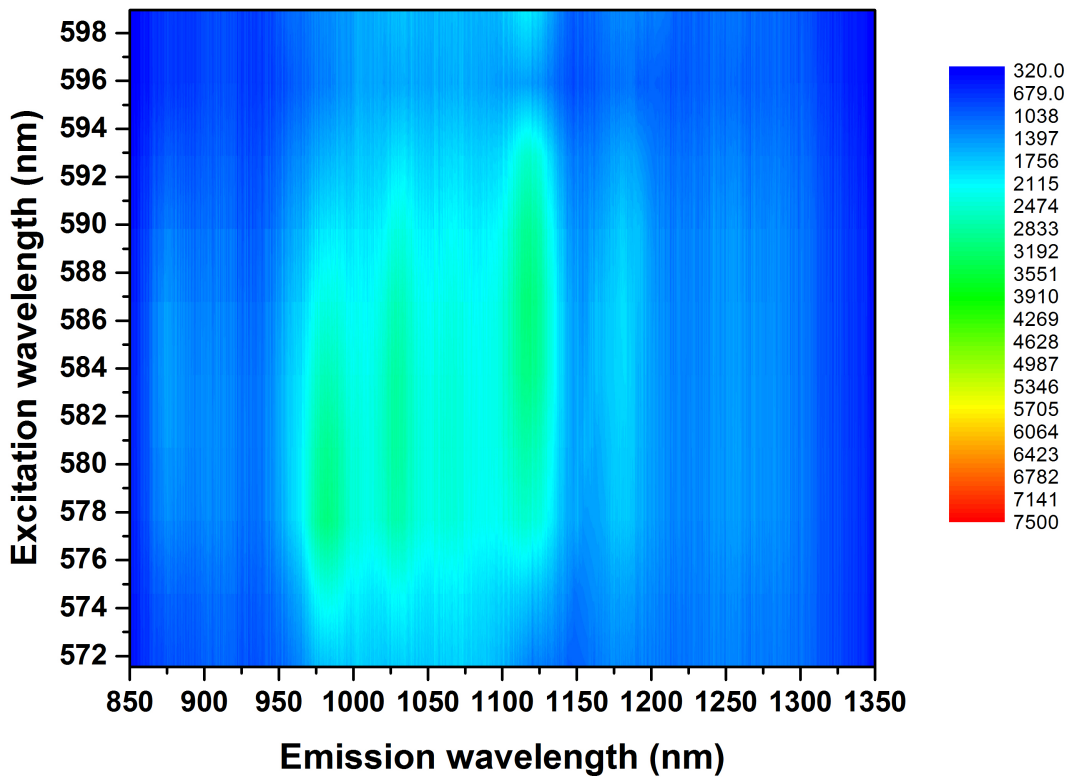


Figure 5.10: Photoluminescence spectroscopy for purified sample. It is not possible to assigned chiral indices to this sample owing to the reduction of fluorescence.

For the assignment of chiral indices, we used the photoluminescence spectroscopy table for SWCNTs [37]. We took into account the approximate values of emission and excitation wavelengths in both samples and we compared them with the values of the table. We observed for non-purified sample that its chiral indices explicitly the semiconducting character of the nanotubes obeying $n - m \neq 3l$.

This results represent the first studies of photoluminescence on B-doped nan-

otubes. Although at this stage, they are not conclusive, this is the matter of ongoing work.

5.5 Final comments

The previous results exhibit that the procedure to characterize the optical responses for CBx-SWCNTs allows us to determine the diameters of the single-walled nanotubes found in our samples. Clearly, we could assign chiral indices for the sample synthesized with 25% of iron nitrate concentration, but the optical absorption and photoluminescence spectroscopy do not allow to come to the same results in terms of chiral indices assigned.

Such result motivates us to further investigate what process must be improved in order to get the same results in terms of chiral indices and approach diameters in our samples for using optical spectroscopy techniques. In spite of the experimental and technical difficulties, we were able to characterize the optical responses of the Boron doped single-walled nanotubes for the first time. The spectroscopy techniques reveal important data about the optical features of the matter in which case for our samples, we observed that the CBx-SWCNTs have more semiconducting than metallic tubes. This is still arguable because the incorporation of boron should increase the population of metallic tubes. However, the well-known metallic quenching for metallic tubes in photoluminescence would not allow to verify their presence.

As mentioned before, the Hybrid Tailored Systems group at University of Vienna, has ongoing researched on the topic and many technical technical aspects that intervene to characterize its optical properties are constantly investigated.

Bibliography

- [1] Stephanie Reich, Christian Thomsen, and Janina Maultzsch. *Carbon Nanotubes: Basic Concepts and Physical Properties*, volume 10. 2004.
- [2] Paola Ayala, Raul Arenal, Annick Loiseau, Angel Rubio, and Thomas Pichler. The physical and chemical properties of heteronanotubes. *Reviews of Modern Physics*, 82:1843–1885, 2010.
- [3] P. Ayala, M. H. Rümmeli, T. Gemming, E. Kauppinen, H. Kuzmany, and T. Pichler. CVD growth of single-walled B-doped carbon nanotubes. *Physica Status Solidi (B)*, 245:1935–1938, 2008.
- [4] Y. F. Li, Y. Wang, S. M. Chen, H. F. Wang, T. Kaneko, and R. Hatakeyama. Electrical transport properties of boron-doped single-walled carbon nanotubes. *Journal of Applied Physics*, 113(5):–, 2013.
- [5] A Jorio, R Saito, G Dresselhaus, and M S Dresselhaus. Determination of nanotubes properties by Raman spectroscopy. *Philosophical transactions. Series A, Mathematical, physical, and engineering sciences*, 362:2311–2336, 2004.
- [6] Jean-Christophe Charlier, Xavier Blase, and Stephan Roche. Electronic and transport properties of nanotubes. *Reviews of Modern Physics*, 79:677–732, 2007.
- [7] Ge G Samsonidze, R Saito, A Jorio, M A Pimenta, A G Souza Filho, A Grüneis, G Dresselhaus, and M S Dresselhaus. The concept of cutting lines in carbon nanotube science. *Journal of nanoscience and nanotechnology*, 3:431–458, 2003.
- [8] Christian Ng and Marcel Van de Voorde. *Nanotechnology in a Nutshell: From Simple to Complex Systems*, chapter 5. New Forms of Carbon and New Opportunities, pages 71–84. Springer-Verlag.
- [9] P. Roche S. Salvétat J Loiseau, A. Petit. *Understanding Carbon Nanotubes: from Basics to Applications*, e-book 2. Synthesis Methods and Growth Mechanics, pages 49–122. Lecture Notes in Physics. Springer-Verlag, New York, October 2005.
- [10] G. Avouris P Dresselhaus, M. Dresselhaus. *Carbon Nanotubes: Synthe-*

- sis, Structure, Properties, and Applications*, volume 80 of *Topic in Applied Physics*, e-book Nanotube Growth and Characterization, pages 29–39. Springer-Verlag, New York, 15 edition, January 2001.
- [11] Peter J.F Harris. *Carbon Nanotubes Science*, chapter 2. Synthesis I: arc-and laser-vaporization, and heat treatment methods, pages 14–38. Cambridge University Press, 2009.
- [12] Peter J.F Harris. *Carbon Nanotubes Science*, chapter 3. Synthesis II: catalytic chemical vapour deposition and related methods, pages 14–38. Cambridge University Press, 2009.
- [13] K. McGuire, N. Gothard, P. L. Gai, M. S. Dresselhaus, G. Sumanasekera, and A. M. Rao. Synthesis and Raman characterization of boron-doped single-walled carbon nanotubes. *Carbon*, 43:219–227, 2005.
- [14] G. Ruiz-Soria, P. Ayala, S. Puchegger, H. Kataura, K. Yanagi, and T Pichler. On the purification of cvd grown boron doped single-walled carbon nanotubes. *physica status solidi (b)*, 248(11):2504–2507, 2011.
- [15] Benoy Anand, Ramakrishna Podila, Paola Ayala, Luciana Oliveira, Reji Philip, S Siva Sankara Sai, Anvar A Zakhidov, and Apparao M Rao. Nonlinear optical properties of boron doped single-walled carbon nanotubes. *Nanoscale*, 5:7271–6, 2013.
- [16] M.S. Dresselhaus, A. Jorio, and R. Saito. *Characterizing Graphene, Graphite, and Carbon Nanotubes by Raman Spectroscopy*, 2010.
- [17] Yuhei Miyauchi. Photoluminescence studies on exciton photophysics in carbon nanotubes. *J. Mater. Chem. C*, 1:6499–6521, 2013.
- [18] C. Maultzsch J Reich, S. Thomsen. *Carbon Nanotubes: Basic concepts and Physical properties*, e-book. 8. Vibrational properties, pages 135–174. Lecture Notes in Physics. Wiley Vch-Verlag, October 2004.
- [19] G. Avouris P Dresselhaus, M. Dresselhaus. *Carbon Nanotubes: Synthesis, Structure, Properties, and Applications*, volume 80 of *Topic in Applied Physics*, e-book Introduction to Carbon Material Research: 1. Historical Introduction, pages 1–8. Springer-Verlag, New York, 15 edition, January 2001.
- [20] P. Roche S. Salvétat J Loiseau, A. Petit. *Understanding Carbon Nanotubes: from Basics to Applications*, e-book 1. Polymorphism and Structure of Carbons, pages 1–43. Lecture Notes in Physics. Springer-Verlag, New York, October 2005.
- [21] R Eisberg and R Resnick. *Quantum Physics of Atoms, Molecules, Solids, Nuclei and Particles*, chapter 7th; One-electron atoms, pages 232–259. John Wiley and Sons, 2nd edition.
- [22] H Ibach, H. Luth. *Solid-State Physics: An introductory to theory and experiment*, chapter 1st; Chemical Bonding in Solids, pages 3–12. Springer, 3th edition, February 2009.

- [23] Online. Quantum mechanics and bonding hybridization. <http://www.dpcdsb.org/NR/rdonlyres/9B6E4EF6-77F0-407F-A858-F0DF78B6896C/106061/46QuantumMechanicsandBondingHybridization.pdf>, 2014. Accessed: 2014-05-10.
- [24] C. Maultzsch J Reich, S. Thomsen. *Carbon Nanotubes: Basic concepts and Physical properties*, e-book. 2. Structure and Symmetry, pages 3–30. Lecture Notes in Physics. Wiley Vch-Verlag, October 2004.
- [25] C Kittel. *Introduction to Solid State Physics*, book. 2nd; Wave Diffraction and Reciprocal Lattice, pages 23–43. Jhon Wiley & Sons, 8th edition, 2004.
- [26] C. Maultzsch J Reich, S. Thomsen. *Carbon Nanotubes: Basic concepts and Physical properties*, e-book. 3. Electronic properties of Carbon Nanotubes, pages 31–64. Lecture Notes in Physics. Wiley Vch-Verlag, October 2004.
- [27] Oleg Starykh. Advanced solid state i:physics of modern materials. <http://www.physics.utah.edu/~starykh/phys7510/>, 2012.
- [28] G. Avouris P Dresselhaus, M. Dresselhaus. *Carbon Nanotubes: Synthesis, Structure, Properties, and Applications*, volume 80 of *Topic in Applied Physics*, e-book Optical properties and Raman Spectroscopy of Carbon Nanotubes, pages 213–244. Springer-Verlag, New York, 15 edition, January 2001.
- [29] H Ajiki and T Ando. Aharonov-Bohm effect in carbon nanotubes. *Physica B: Condensed Matter*, 201:349–352, 1994.
- [30] Ruchita S. Das and Y.K. Agrawal. Raman spectroscopy: Recent advancements, techniques and applications, 2011.
- [31] Peter J. F.. Harris. Cambridge University Press, 2009.
- [32] Zhuang Liu, Scott Tabakman, Kevin Welsher, and Hongjie Dai. Carbon nanotubes in biology and medicine: In vitro and in vivo detection, imaging and drug delivery. *Nano Research*, 2:85–120, 2009.
- [33] Ivo Stemmler and Claudia Backes. Absorption spectroscopy as a powerful technique for the characterization of single-walled carbon nanotubes. http://www.perkinelmer.com/CMSResources/Images/44-156326WHT_011513_01_LAMBDA_1050Single-WalledCarbonNanotubes.pdf, 2014. Accessed: 2014-05-10.
- [34] Wikipedia. Cntn absorption. http://en.wikipedia.org/wiki/Optical_properties_of_carbon_nanotubes#mediaviewer/File:CNTabsorption.jpg, 2014. Accessed: 2014-06-14.
- [35] H. Kataura, Y. Kumazawa, Y. Maniwa, I. Umezue, S. Suzuki, Y. Ohtsuka, and Y. Achiba. Optical properties of single-wall carbon nanotubes. *Synthetic Metals*, 103:2555–2558, 1999.
- [36] F. Bonaccorso, T. Hasan, P. H. Tan, C. Sciascia, G. Privitera, G. Di Marco, P. G. Gucciardi, and A. C. Ferrari. Density gradient ultracentrifugation of

- nanotubes: Interplay of bundling and surfactants encapsulation. *Journal of Physical Chemistry C*, 114:17267–17285, 2010.
- [37] Sergei M. Bachilo, Michael S. Strano, Carter Kittrell, Robert H. Hauge, Richard E. Smalley, and R. Bruce Weisman. Structure-assigned optical spectra of single-walled carbon nanotubes. *Science*, 298(5602):2361–2366, 2002.

PERSONAL DETAILS

Name: Harvey Andrés Suárez Moreno
Date of birth: 10.10.1984
Place of birth: Bogotá, Colombia
Current address: Hagenmuellergasse 31, Zimmer 308, 1030-Vienna, Austria
Marital status: Single
Mobile: 0681201252
email: a1149889@unet.univie.ac.at

EDUCATION

2014 Candidate to Master of Science in Physics, University of Vienna. Thesis: Optical Characterization of Boron doped Single-Walled Carbon Nanotubes. Supervisor: Univ.Prof. Dr. Paola Ayala
2010 Bachelor of Physics, Pedagogical National University. Thesis: Quantum correlation; central topic for an introductory course of quantum mechanics. Supervisor: Univ. Prof. Dr. Jose Orlando Organista Rodriguez
2005 Technician lathe and milling machine. Sena: workshop practicing in fabrication of mechanical components for industry. Supervisor: Prof. Eng. Daniel Tovar
2001 Technical high school. Inem Kennedy

RESEARCH INTERESTS

- Quantum theory since point of view information theory
- Quantum Nanophysics related to the production of Carbon nanotubes construction
- Spectroscopy techniques
- Foundations and experiments in quantum theory

TEACHING ASSISTANT

Pedagogical National University of Colombia
2008-2009 Teaching assistant
Integer and differential calculus, Physics II

FELLOWSHIPS AND GRANTS

2012-2014 Colfuturo-Futuro para Colombia: Founding for studies abroad.

PROFESSIONAL EXPERIENCE

Consultant documentary in Natural Science Education, *Pedagogical National University*, 2010

PUBLICATIONS

Act to measurement in the microscopical world: a material for teaching and understanding. In Revista Colombiana de Física (RCF). Vol 43, No 3. Pg 583. ISSN: 0120-2650. October of 2011 by H. Surez, J. Organista and D. Duque.

MEETINGS AND WORKSHOPS

- Conference "Quantum [Un]Speakables II" 50 years of Bell's Theorem, Austria. June 19-22nd, 2014
- Workshop "Quantum physics and information", Traunkirche, Austria. April 9th of 2012. Contribution "Report about the quantum effects in LC circuits"
- XXIII National Congress of Physics. Santa Marta (Magdalena), Colombia. October 5th to 9th of 2009. Speaker "Act to measurement in the microscopical world: a material for teaching and understanding".
- IX Interamerican Congress to Physics Teaching. Rionegro (Antioquia), Colombia. July 2nd to 6th of 2009. Speaker with poster "Some epistemological assumptions underlying

the ideas of quantum physics and its importance in the formation of physics teachers”.

COMPUTATIONAL SKILLS

- Tex editor:
TeXworks, Scientific Workplace 5.5, Winedt 7
- SO-OS:
Office windows, Mac-OSX, Linux (basics), Matlab, Derive, Cabri 3D, Origin 7-8 version
- Programming Language:
C++(Basics), HiQ-5, Labview (Basics), NI Instruments Electronic workbench

LANGUAGES

- Spanish; mother tongue
- English-Fluent
- German; written and spoken good